AD-A089 099 PENNSYLVANIA STATE UNIV UNIVERSITY PARK APPLIED RESE--ETC F/G 7/4
AN INVESTIGATION OF THE HEAT TRANSFER AT THE LIQUID/SOLID INTER--ETC(U)
MAR 80 J E FREDLEY N00024-79-C-6043
UNCLASSIFIED ARL/PSU/TM-80-94 NL

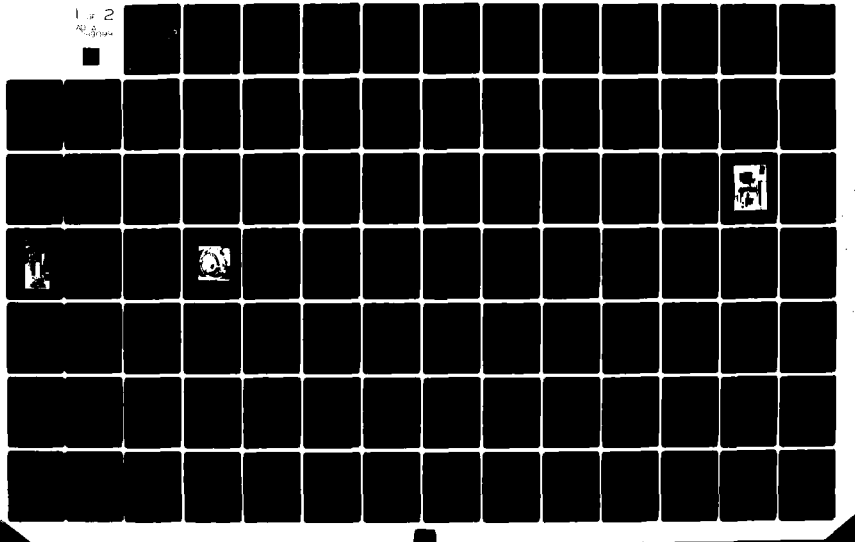

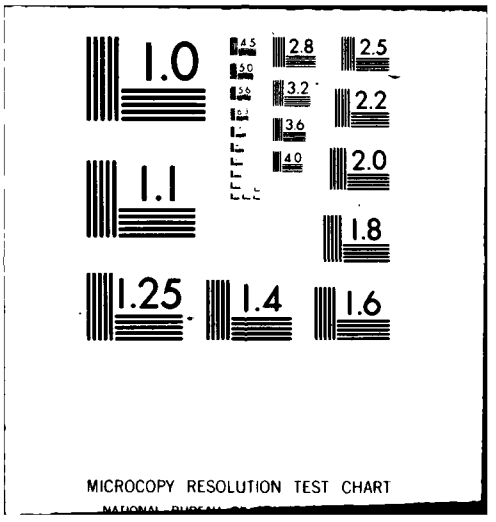
1.0
1.1
1.25
1.4
1.6
1.8
2.0
2.2
2.5
2.8
3.2
3.6
4.0
4.5
5.0
5.6
MICROCOPY RESOLUTION TEST CHART

12

AN INVESTIGATION OF THE HEAT TRANSFER AT THE LIQUID/SOLID INTERFACE OF RAPIDLY MELTING ICE

Joseph Edward Fredley

Technical Memorandum
File No. TM 80-94
March 25, 1980
Contract No. N00024-79-C-6043

Copy No. 5

The Pennsylvania State University
Intercollege Research Programs and Facilities
APPLIED RESEARCH LABORATORY
Post Office Box 30
State College, PA 16801

NAVY DEPARTMENT

NAVAL SEA SYSTEMS COMMAND

UNCLASSIFIED

SECURITY CLASSIFICATION OF THIS PAGE (When Data Entered)

(12) 102

REPORT DOCUMENTATION PAGE

READ INSTRUCTIONS BEFORE COMPLETING FORM

(14) ARL/PSU TM-80-94

2. GOVT ACCESSION NO. AD-A089 099

3. RECIPIENT'S CATALOG NUMBER

4. TITLE (and Subtitle) (6)

AN INVESTIGATION OF THE HEAT TRANSFER AT THE LIQUID/SOLID INTERFACE OF RAPIDLY MELTING ICE

5. TYPE OF REPORT & PERIOD COVERED

MS Thesis, May 1980

6. PERFORMING ORG. REPORT NUMBER

TM 80-94

7. AUTHOR(s) (10)

Joseph Edward Fredley

8. CONTRACT OR GRANT NUMBER(s) (15)

N00024-79-C-6043

9. PERFORMING ORGANIZATION NAME AND ADDRESS

The Pennsylvania State University
Applied Research Laboratory
P. O. Box 30, State College, PA 16801

10. PROGRAM ELEMENT, PROJECT, TASK AREA & WORK UNIT NUMBERS

11. CONTROLLING OFFICE NAME AND ADDRESS

Naval Sea Systems Command
Department of the Navy
Washington, DC 20362

(11) 25

12. REPORT DATE

March 1980

13. NUMBER OF PAGES

100 pages & figures

14. MONITORING AGENCY NAME & ADDRESS(if different from Controlling Office) (9) Masters Thesis

15. SECURITY CLASS. (of this report)

Unclassified, Unlimited

15a. DECLASSIFICATION/DOWNGRADING SCHEDULE

16. DISTRIBUTION STATEMENT (of this Report)

Approved for public release, distribution unlimited, per NSSC (Naval Sea Systems Command), 5/14/80

17. DISTRIBUTION STATEMENT (of the abstract entered in Block 20, if different from Report)

18. SUPPLEMENTARY NOTES

19. KEY WORDS (Continue on reverse side if necessary and identify by block number)

ice, water, melting, thesis

20. ABSTRACT (Continue on reverse side if necessary and identify by block number)

This paper describes an experimental and analytical investigation of a system capable of rapidly melting ice. The melting technique used involved forcing a cylindrical ice slug against a heated surface, letting the effluent fluid exit radially. An analytical model based on fundamental physical principles was developed and used to predict the behavior of the system. Liquid layer thickness, liquid bulk temperature, radial pressure distribution

DD FORM 1 JAN 73 1473 EDITION OF 1 NOV 65 IS OBSOLETE
S/N 0102-LF-014-6601

391007

UNCLASSIFIED

SECURITY CLASSIFICATION OF THIS PAGE (When Data Entered)

20. ABSTRACT (continued)

in the liquid layer, convective heat transfer coefficient, and ice melt rate were all computed for steady state operation of the system.

Experiments were performed to verify the model predictions. The tests measured the ice melt velocity and exit bulk temperature at a known supply pressure. The input heat flux was determined using two independent methods of calculation. One technique found the conduction heat flux leaving the heated block by using two heated block temperature measurements spaced a known distance apart near the liquid/block surface. The second method applied the measured ice melt velocity and liquid bulk temperature to an energy balance on the liquid film to yield an input heat flux value. A comparison of the experimental results with the analytical model predictions is made demonstrating satisfactory agreement.

ABSTRACT

Described in this paper is an experimental and analytical investigation of a system capable of melting ice rapidly. The melting technique used involves forcing a cylindrical ice slug against a heated surface and letting the effluent fluid exit radially. An analytical model based on fundamental physical principles is developed and used to predict the behavior of the system. Liquid layer thickness, liquid bulk temperature, radial pressure distribution in the liquid layer, convective heat transfer coefficient, and ice melt rate are computed for steady state operation of the system.

Experiments were performed verifying the model predictions. The tests measured the ice melt velocity and exiting liquid bulk temperature at a known supply pressure. The input heat flux is determined by use of two independent methods of calculation: (1) finding the conduction heat flux leaving the heated block by use of two heated block temperature measurements spaced a known distance apart near the liquid/block surface and (2) applying the measured ice melt velocity and liquid bulk temperature to an energy balance on the liquid film. A comparison of the experimental results with the analytical model predictions is made and demonstrates satisfactory agreement.

TABLE OF CONTENTS

	Page
ABSTRACT	iii
LIST OF FIGURES	vi
LIST OF TABLES	viii
LIST OF SYMBOLS	ix
ACKNOWLEDGEMENTS	xiii
I. INTRODUCTION	1
1.1 General Statement of the Problem	1
1.2 Previous Related Studies	4
1.3 Scope and Objectives of the Present Work	5
II. ANALYTICAL CONSIDERATIONS	6
2.1 Analytical Model	6
2.2 Continuity	9
2.3 First Law of Thermodynamics	10
2.4 Heat Transfer Equations	14
2.5 Momentum Equation	15
2.6 Solution Technique	22
III. EXPERIMENTAL INVESTIGATION	24
3.1 Experimental Concept	24
3.2 Apparatus	24
3.3 Instrumentation	35
3.4 *Test Procedure*	38
IV. RESULTS AND DISCUSSION	43
4.1 Experimental Results	43
4.2 Analytical Results	61
4.3 Experimental-Analytical Comparisons	70
V. CONCLUSIONS AND RECOMMENDATIONS FOR FUTURE WORK	75
BIBLIOGRAPHY	79

Page

APPENDIX A: DERIVATION OF THE POLYNOMIAL APPROXIMATIONS FOR THE KINEMATIC VISCOSITY, DENSITY, AND THERMAL CONDUCTIVITY OF WATER AS A FUNCTION OF LIQUID BULK TEMPERATURE 82

APPENDIX B: TABULATION OF THE RAW TEST DATA 84

LIST OF FIGURES

Figure		Page
1.	Cutaway View of the Test Specimen Assembly	3
2.	General System Geometry	7
3.	Liquid Film Control Volume	8
4.	Solid Ice Control Volume	12
5.	Liquid Film Control Volume Showing Forces	16
6.	Top View of the Liquid Film Control Volume Showing Forces	17
7.	Flow Chart for the Computational Procedure	23
8.	Photograph of the Complete Test Facility	25
9.	Schematic of the Test Facility	26
10.	Photograph of the Test Specimen Assembly	27
11.	Photograph of the Assembled Hot Block and Collar	30
12.	Schematic of the Pressure Control System	33
13.	Supply Pressure Calibration Curve	34
14.	Schematic of the Instrumentation System	36
15.	Thermocouple Placement	37
16.	Schematic of the Temperature Measurement Calibration . .	39
17.	Experimental Results, V_s versus $\dot{Q}''_k$	50
18.	Experimental Results, V_s versus $\dot{Q}''_t$	51
19.	Experimental Results, T versus $\dot{Q}''_k$	52
20.	Experimental Results, T versus $\dot{Q}''_t$	53

Figure		Page
21.	Thermocouple Placement and Cavity Concept	56
22.	Analytical Results, V_s versus $\dot{Q}''_i$	65
23.	Analytical Results, T versus $\dot{Q}''_i$	66
24.	Predicted Pressure Distribution, P_s = 2.592 MPa $\dot{Q}''_i$ = 3.785 MW/m^2	68
25.	Pressure versus Saturation Temperature for Water	69
26.	Experimental-Analytical Comparisons, V_s versus $\dot{Q}''_k$	71
27.	Experimental-Analytical Comparisons, V_s versus $\dot{Q}''_t$	72
28.	Experimental-Analytical Comparisons, T versus $\dot{Q}''_k$	73
29.	Experimental-Analytical Comparisons, T versus $\dot{Q}''_t$	74

LIST OF TABLES

Table		Page
1.	Recorded Test Data	41
2.	Experimental Test Matrix	44
3.	Reduced Data, P_s = 1.269 MPa	47
4.	Reduced Data, P_s = 2.592 MPa	48
5.	Reduced Data, P_s = 3.606 MPa	49
6.	Constant Input Data	62
7.	Analytical Test Matrix, Input Data	63
8.	Output Data List	64
B-1.	Raw Test Data, P_s = 1.269 MPa	85
B-2.	Raw Test Data, P_s = 2.592 MPa	86
B-3.	Raw Test Data, P_s = 3.606 MPa	87

LIST OF SYMBOLS

Symbol	Description
A_r	liquid layer area normal to radial flow (m^2)
A_s	top surface area of the liquid control volume in Figure 3 (m^3)
A_s'	top surface area of the liquid control volume in Figure 5 (m^2)
C_p	specific heat of liquid at constant pressure ($J/g-^oC$)
C_{ps}	specific heat of solid at constant pressure ($J/g-^oC$)
D_h	hydraulic diameter for the liquid film (m)
F	side force on liquid in Figure 5 (N)
F_f	frictional force (N)
F_r	radial force at some radial position r (N)
F_r'	radial component of the liquid side force (N)
F_u	upward force on the ice caused by liquid film (N)
f_r	friction factor
$\dot{H}$	rate change in total enthalpy of the solid (W)
$h_r = h$	convective heat transfer coefficient at radial position r (W/m^2-^oC)
h_l	enthalpy of liquid leaving control volume in Figure 4 (J/g)
h_s	enthalpy of the solid (J/g)

Symbol	Description
$\dot{h}_s$	rate change in enthalpy of the solid (W/g)
h_{sf}	latent heat of fusion (J/g)
k	thermal conductivity of the hot block (W/m-^{o}C)
k_r	thermal conductivity of the liquid (W/m-^{o}C)
M_s	total mass of the solid (g)
$\dot{M}_s$	rate change in mass of the solid (g/sec)
$\dot{m}_m$	mass flow rate of liquid entering liquid control volume in Figure 3 (g/sec)
$\dot{m}_r$	mass flow rate of liquid at radial position r (g/sec)
Nu_r	Nusselt number at radial position r
P_r	liquid pressure at radial position r (Pa)
$\dot{Q}''_i$	constant input heat flux (W/m^2)
$\dot{Q}''_k$	constant input heat flux as measured in the hot block (W/m^2)
$\dot{Q}''_m$	heat flux from the liquid layer to the ice (W/m^2)
$\dot{Q}''_t$	constant input heat flux as determined from conservation of energy (W/m^2)
Re_r	Reynolds number at radial position r
r	radial distance from the centerline (m)
r_e	exit radius of the liquid film (m)
T_c	liquid bulk temperature at the centerline (^{o}C)

Symbol	Description
T_e	liquid bulk temperature at the exit radius (^oC)
T_m	melting temperature of the solid at standard pressure (^oC)
$T_r = T$	liquid bulk temperature at radial position r (^oC)
T_s	initial solid temperature (^oC)
$\dot{T}_s$	rate change in temperature of the solid (^oC/sec)
ΔT	temperature difference measured in hot block (^oC)
t	event time during experimental tests (sec)
$\dot{U}$	rate change in internal energy of the solid (W)
U_s	internal energy of the solid control volume in Figure 4 (J/g)
$\dot{V}$	rate change in volume of the solid (m^3/sec)
V_r	average liquid radial velocity at radial position r (m/sec)
V_s	downward solid velocity (m/sec)
z	ramrod position (m)
ΔZ	thermocouple spacing in the hot block (m)

Greek Letters

δ_c	liquid film thickness at the centerline (m)
δ_e	liquid film thickness at the exit radius (m)
$\delta_r = \delta$	liquid film thickness at radial position r (m)
ν	liquid kinematic viscosity (m^2/sec)

Greek Letters	Description
$\rho_r = \rho$	liquid density (g/m^3)
ρ_s	solid density (g/m^3)
τ_r	wall shear stress at radial position r (Pa)
θ	elemental angle for control volumes (radians)

ACKNOWLEDGEMENTS

The author would like to express his appreciation for the professional counsel provided by Professor C. H. Wolgemuth and Dr. T. G. Hughes. The free exchange of questions, suggestions, and advice in the many thesis discussions created sustaining interest and nurtured a growth of insight into the problem that was invaluable to the eventual completion of this research.

The author is also appreciative of the support obtained from the Applied Research Laboratory of The Pennsylvania State University under contract with the Naval Sea Systems Command and from Professor M. T. Pigott in particular for his role in monitoring this study as part of the Exploratory and Foundational Research program.

CHAPTER I

INTRODUCTION

1.1 General Statement of the Problem

Rankine cycle systems normally use a working fluid that exists as a liquid at standard conditions. Water is the most commonly used fluid because of its vapor pressure characteristics (the temperatures and pressures at which it boils and condenses); its low cost; its safety (toxicity, corrosiveness, and flammability); and its generally very good thermodynamic performance characteristics. When the system must be stored in subfreezing environments, freezing of the working fluid becomes a problem. In such applications, either alternate working fluids must be used or if water is to be used the freezing problem must be solved.

Additives are available which will prevent the water from freezing but which have the general disadvantages of reducing system performance if left in place or complicating the machinery if removed after startup. A considerable body of knowledge has been accumulated on alternate working fluids since the United States Environmental Protection Agency (EPA) has funded work on Rankine cycle systems for automotive applications. Most of the alternate working fluids which these studies have considered are organic fluids incapable of withstanding high cycle temperatures. Organic fluids thermally decompose when exposed to high temperatures. If the peak temperatures are reduced to avoid this problem, the performance of the system is significantly degraded.

(Ideal cycle efficiency is directly related to peak temperature.) These organic fluids are also expensive and, in most cases, toxic and/or flammable and/or corrosive. After screening 112 candidate fluid constituents and binary and ternary mixtures of some of these, the two fluids chosen by a Sundstrand study (1) as worthy of further consideration are toxic, flammable, and somewhat corrosive. A similar independent study by Wolgemuth (2) (more than 50 articles in the literature were reviewed and over 107 fluids were examined) yielded only three "satisfactory" candidate working fluids; however, all of these are either toxic, corrosive, or flammable. Thus, of the presently available working fluids, water remains the most suitable for typical Rankine cycle applications.

When it is assumed that it is not feasible for the system environment to be kept above the freezing temperature with the use of heating equipment, a possible solution to the freezing problem is the storage of the working fluid in a reservoir where freezing is permitted to occur. This is acceptable as long as the working fluid can be melted and delivered to the system at the required rates upon startup. This work has been directed toward studying this melting process. The results are directly applicable to small Rankine power systems capable of several hundred kilowatts.

One possible system configuration proposed allows the water to freeze in a cylindrical accumulator shown schematically in Figure 1. The cylinder is modified so that a hot block may be mounted on one end with appropriate ports for removing the liquid formed when the ice is melted. The hot block may be heated rapidly upon system startup by use of a variety of techniques including the combustion of propellants or other chemicals in the block, resistance heating, or induction heating.

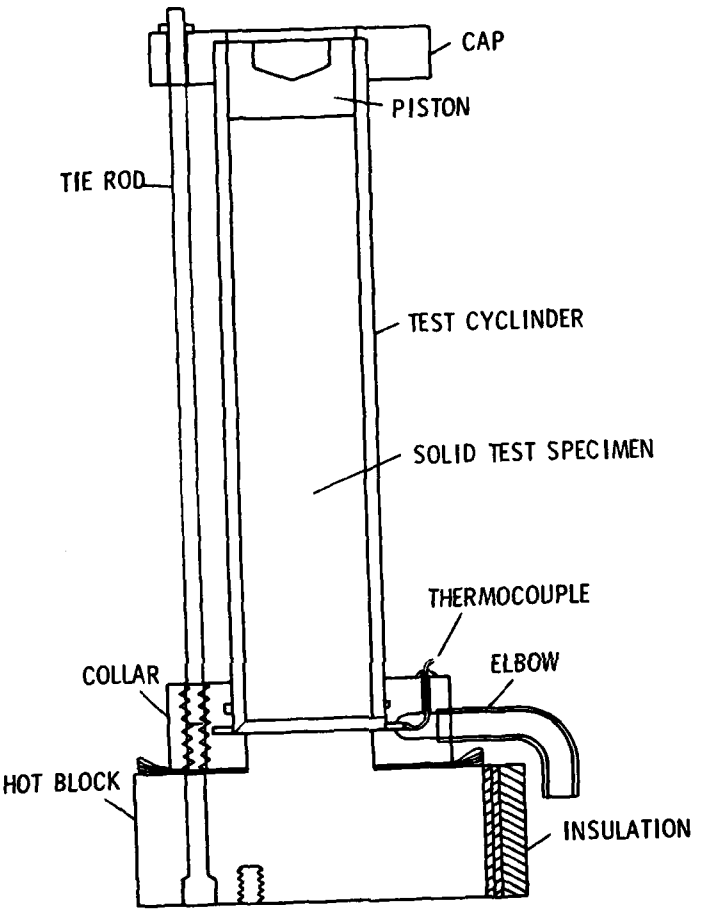

Figure 1. Cutaway View of the Test Specimen Assembly.

The selected process needs to be very rapid and a chemical reaction is the most likely candidate. At the same time, pressure is applied to the ice cylinder and continually forces it against the heated block where it is melted. The liquid formed on melting flows radially from the interface and exits from ports in the accumulator.

1.2 Previous Related Studies

Many techniques have been devised for the analytical and numerical solution to the general melting solid heat transfer problem. Ablation problems, those in which the molten substance is blown away immediately upon formation, are similar to the one under study except that there is no treatment of the liquid film per se. Solutions for ablating solids are numerous. Bankoff (3), Holman (4), Landau (5), and Lotkin (6) offer examples of these solutions. Solidification and melting processes have also been studied for flow between parallel surfaces. Musman (7); Yen (8, 9); and Moore (10) investigated these processes where convective mixing took place in a liquid film moving slowly between surfaces whose separation distance is much larger than the liquid film thickness envisioned in this study. Yen (11), in a later paper, examined ice melting in a system where the liquid was not removed upon formation which created an increasingly thick liquid layer between the ice and the heat source. Transient melting behavior has also been studied. Numerical solutions for the transient behavior have been developed by Bowley (12), Friedman (13), Murray and Landis (14), and Nansteel (15) for moving boundary systems involving solidification of the liquid in its flow passage. Kreith and Romie (16) examined the melting of a semi-infinite solid, a cylinder, and a sphere and determined the position of the

solid-liquid interface and the surface temperature-time history for substances initially at the fusion temperature. Tien and Yen (17) modeled a drifting iceberg in sea water to determine the effect of melting on the convective heat transfer coefficient. Their results for laminar flow indicated that melting inhibits the heat transfer rate. Masters (18) studied the effects of intense surface heating on a slab. An ablation solution was used to set an upper solution bound for the melting rate. When liquid removal only by evaporation was assumed, a lower bound was formulated. All of these studies, however, do not examine the melting system of this study. The proposed melting technique in the indicated geometry has not yet been investigated.

1.3 Scope and Objectives of the Present Work

This study examines the processes occurring at the melting interface to determine the melting potential for a system of the general configuration of Figure 1. To these ends, two actions were taken:

1. An analytical model for the melting interface was developed and solved over a range of conditions to predict the behavior of melting ice under the conditions of this study.
2. Experiments were performed using the melt system of Figure 1 and the test data compared to the analytical model.

CHAPTER II

ANALYTICAL CONSIDERATIONS

2.1 Analytical Model

The basic geometry of the system is shown in Figure 2. A thin liquid film is assumed to exist between the hot block and the solid cylinder of ice. The solid ice cylinder is moved downward by a known force as the solid melts while the liquid produced by the melting solid flows radially outward between the two solid surfaces. Heat is transferred axially from the hot block through the liquid film to the melting solid.

Equations for the liquid velocity, the liquid film thickness, the liquid temperature and pressure, and the melting rate were obtained from expressions for the conservation of mass, the first law of thermodynamics, the conservation of momentum, and a convective heat transfer relationship.

The analytical model was developed for steady flow conditions in the liquid film. The control volume chosen for analysis is shown in Figure 3. While the problem is not truly a steady state problem (the hot block temperature decreases with time), experiments have shown that a relatively long period of time exists where the melt rate is approximately constant. The heat flux from the hot block to the liquid was therefore assumed to be a constant uniform heat flux. Additional assumptions made concerning the development of the descriptive equations for the liquid control volume are summarized as follows:

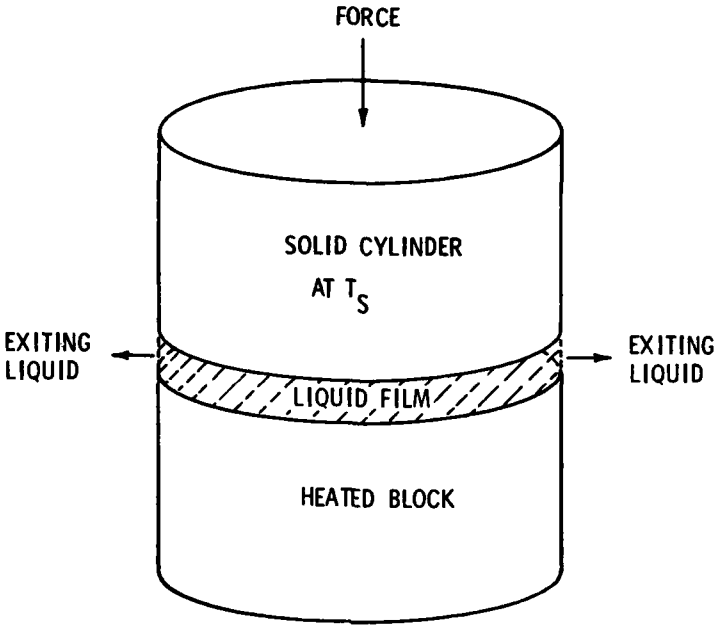

Figure 2. General System Geometry.

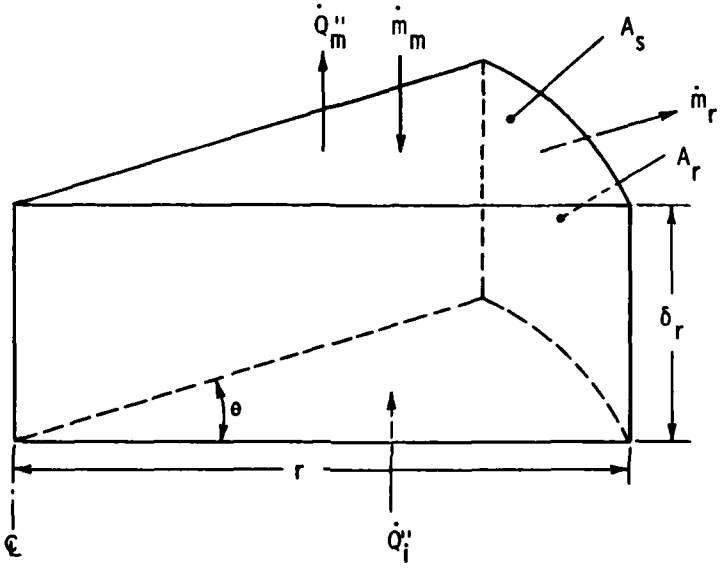

Figure 3. Liquid Film Control Volume.

1. At any given location within the control volume, none of the variables ($\dot{m}_m$, $\dot{m}_r$, $\dot{Q}''_m$, and $\dot{Q}''_i$) vary with time (see Figure 3).
2. The substance under investigation is distilled water and contains no dissolved air. Pressure effects on the water's thermal properties are considered negligible.
3. The bulk temperature of the solid approaching the melt zone describing the solid's thermal properties is considered to be $-17.8^{o}C$ ($0^{o}F$).
4. The liquid constant pressure specific heat is defined at a nominal liquid bulk temperature of $10^{o}C$ ($50^{o}F$).
5. The radial liquid flow in the control volume is laminar, incompressible, and fully developed.
6. The melting solid and the heated block surfaces are parallel.
7. The flow is considered to be one-dimensional in the radial direction and the heat transfer is considered to be one-dimensional in the axial direction.
8. The kinetic and potential energy for the liquid film control volume are negligible in comparison to the other terms in the energy equation.

2.2 Continuity

Conservation of mass applied to the control volume in Figure 3 with the assumption of steady flow yields

$$\dot{m}_m = \dot{m}_r \quad . \tag{1}$$

Assuming uniform properties over the control surfaces where fluid enters and leaves permits the flow rate to be expressed as

$$\dot{m} = \rho A V \quad . \tag{2}$$

The exiting mass flow rate $\dot{m}_r$ can then be expressed as

$$\dot{m}_r = \rho_r V_r r \theta \delta_r \quad . \tag{3}$$

The mass flow rate of the liquid entering the control volume $\dot{m}_m$ can be expressed as the rate at which the solid melts, which is the rate at which the solid travels downward since δ_r does not change with time. Thus,

$$\dot{m}_m = \rho_s A_s V_s = \rho_s V_s \frac{\theta}{2\pi} \pi r^2 = \rho_s V_s \theta \frac{r^2}{2} \quad . \tag{4}$$

The velocity of the fluid at any radius r can then be obtained from

$$\dot{m}_r = \dot{m}_m = \rho_r V_r r \theta \delta_r = \rho_s V_s \frac{\theta r^2}{2} \tag{5}$$

as

$$V_r = \frac{\rho_s V_s r}{2 \rho_r \delta_r} \quad . \tag{6}$$

2.3 First Law of Thermodynamics

The general form of the first law of thermodynamics applicable to the control volume in Figure 3 can be written as

$$\dot{Q} - \dot{W} = \left(\dot{m}(h + ke + pe)\right)_{out} - \left(\dot{m}(h + ke + pe)\right)_{in} + \dot{E} \quad . \qquad (7)$$

With the assumptions of steady state and no work and negligible changes in kinetic and potential energy, the first law equation becomes

$$(\dot{Q}''_i - \dot{Q}''_m)A_s = (\dot{m}h)_r - (\dot{m}h)_m \quad . \qquad (8)$$

Defining the mass flow rates by use of Equation (3) and also defining the enthalpy difference as the product of the constant pressure specific heat of the liquid and the increase in liquid bulk temperature above the melting temperature yields

$$(\dot{Q}''_i - \dot{Q}''_m)\frac{\pi r^2 \theta}{2\pi} = \rho_r A_r V_r C_p (T_r - T_m) \quad . \qquad (9)$$

When a substitution for A_r and V_r (Equation (6)) is made and reduced, this equation becomes

$$\dot{Q}''_i - \dot{Q}''_m = \rho_s V_s C_p (T_r - T_m) \quad . \qquad (10)$$

Solving for the liquid bulk temperature yields

$$T_r = \frac{\dot{Q}''_i - \dot{Q}''_m}{\rho_s V_s C_p} + T_m \quad . \qquad (11)$$

Applying the general form of the first law, Equation (7), to the solid ice control volume in Figure 4 (note that the steady state assumption does not apply to this control volume) yields

$$\dot{Q}_m = \dot{m}_m h_1 + \dot{U} + P\dot{V} \quad . \qquad (12)$$

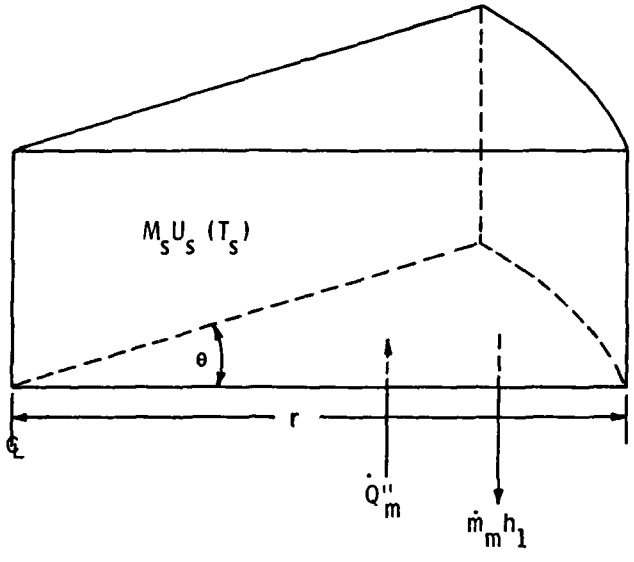

Figure 4. Solid Ice Control Volume.

For this control volume,

$$\dot{U} + P\dot{V} = \dot{H} = \dot{M}_s h + M_s \dot{h} \quad . \tag{13}$$

which when applied to the first law equation yields

$$\dot{Q}_m = \dot{m}_m h_l + \dot{U} + P\dot{V} = \dot{m}_m h_l + \dot{M}_s h_s + M_s \dot{h}_s \quad . \tag{14}$$

Applying conservation of mass to the control volume results in

$$\dot{M}_s = \dot{m}_{in} - \dot{m}_{out} = -\dot{m}_m \quad . \tag{15}$$

Substitution into Equation (14) yields

$$\dot{Q}_m = \dot{m}_m h_{sf} + M_s \dot{h}_s = \dot{m}_m h_{sf} + M_s C_{ps} \dot{T}_s \quad . \tag{16}$$

When it is assumed that the solid is heated from T_s to T_m just before it melts,

$$M_s C_{ps} \dot{T}_s = \dot{m}_m C_{ps} (T_m - T_s) \quad . \tag{17}$$

Substituting this into Equation (16) and expressing the mass flow rate as the product of the solid density, area, and velocity yields

$$\dot{Q}''_m = \rho_s V_s \left(h_{sf} + C_{ps}(T_m - T_s)\right) \quad . \tag{18}$$

Substituting this expression into Equation (11) yields

$$T_r = \frac{\dot{Q}''_i}{\rho_s V_s C_p} - \frac{h_{sf}}{C_p} - \frac{C_{ps}}{C_p}(T_m - T_s) + T_m \quad . \tag{19}$$

2.4 Heat Transfer Equations

Heat is transferred by convection from the liquid film to the solid ice at its melting temperature; hence,

$$\dot{Q}''_m = h_r(T_m - T_r) \quad . \tag{20}$$

Equating Equations (18) and (20) and solving for the convective heat transfer coefficient yields

$$h_r = \frac{\rho_s V_s \left(h_{sf} + C_p(T_m - T_s)\right)}{T_r - T_m} \quad . \tag{21}$$

An analytical heat transfer relationship for fully developed laminar incompressible flow between two parallel plates (19) is given as

$$Nu_r = \frac{5.385}{1 - 0.346(\dot{Q}''_i/\dot{Q}''_m)} \tag{22}$$

where

$$Nu_r = \frac{h_r \delta_r}{k_r} \quad . \tag{23}$$

Equation (22) describes the Nusselt number at the ice/liquid interface. The boundary conditions for the expression consider a constant heat flux into the liquid film from the heated copper block ($\dot{Q}''_i$) and a heat flux leaving the liquid and entering the ice as expressed in Equation (20).

The application of Equation (22) is not exactly correct for the conditions of this study. The liquid flow in Figure 3 is primarily radially outward with axial mass addition occurring at the solid/liquid

interface and thus is not truly fully developed flow between parallel plates. The relationship should, however, provide a reasonable approximation since the heat transfer across the liquid film is actually a conduction process for laminar flow and not a function of the liquid velocity. It is, however, dependent upon the liquid film thickness instead. Solving for the liquid film thickness yields

$$\delta_r = \frac{5.385(k_r)}{h_r\left((1 - 0.346(\dot{Q}''_i/\dot{Q}''_m)\right)} \quad . \tag{24}$$

A close examination of the equation for T_r, (Equation (19), shows that it is not a function of r, since the solid properties do not vary with r and in steady state the solid surface moves downward at a uniform rate. Since T_r is independent of r, inspection of Equation (21) reveals that h_r is also independent of r. With the bulk fluid temperature independent of r, the other liquid properties which are functions of temperature are also independent of r. This fact, in addition to the radial independence of the convective heat transfer coefficient, also indicates in Equation (24) that the liquid film thickness δ_r is independent of r. There is, therefore, no longer any need to use the subscript r on either T, h, or δ.

2.5 Momentum Equation

The pressure of the liquid is a function of r as will be demonstrated by the equation derived from the conservation of momentum. The liquid film control volumes for this analysis are shown in Figures 5 and 6. Conservation of momentum in the radial direction applied to Figure 5 yields

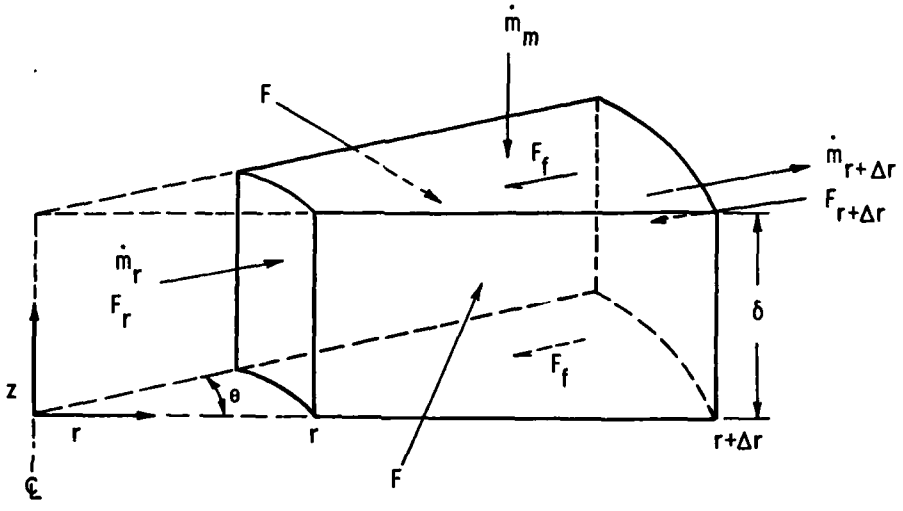

Figure 5. Liquid Film Control Volume Showing Forces.

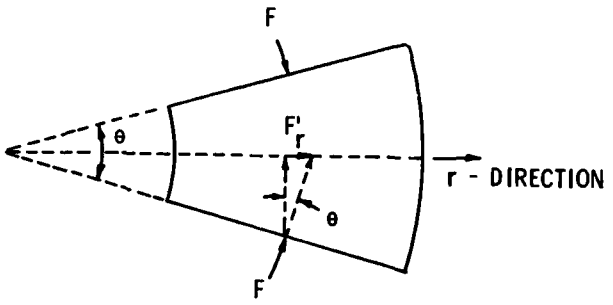

Figure 6. Top View of the Liquid Film Control Volume Showing Forces.

$$F_r + (\dot{m}V)_r + 2F'_r = 2F_f + F_{r+\Delta r} + (\dot{m}V)_{r+\Delta r} \quad . \tag{25}$$

Figure 6 is a top view of the control volume and illustrates more clearly the direction and influence of the side force F. As seen in the figure, the radial component of F can be expressed in terms of the elemental angle and the side force yielding

$$F'_r = F \sin \frac{\theta}{2} \quad . \tag{26}$$

The side force F can be written as the product of an average pressure acting over the area of the control volume side surface and can be expressed as

$$F = PA = \left(\frac{P_r + P_{r+\Delta r}}{2}\right)\Delta r \delta \quad . \tag{27}$$

With second order terms neglected, Equation (26) can then be rewritten as

$$F'_r = P_r \Delta r \delta \sin \frac{\theta}{2} \quad . \tag{28}$$

The frictional force F_f can be expressed as the product of the average wall shear stress and the surface area over which this stress acts. Thus,

$$F_f = \bar{\tau} A'_s = \left(\tau_r + \frac{\Delta \tau}{2}\right)\left(\theta\left(r + \frac{\Delta r}{2}\right)\Delta r\right) \quad , \tag{29}$$

which simplifies to

$$F_f = \tau_r \theta r \Delta r \tag{30}$$

when second order terms are neglected. Approximations for the wall shear stress and friction factor relationships can be obtained by use of available expressions applicable to similar flow conditions. Since the liquid film thickness is expected to be very small in comparison to the circumference at the test cylinder (analytical model predicts 1:9800), a parallel plates geometry can be assumed. The wall shear stress can be expressed in terms of the friction factor and the velocity, Reference (20), as

$$\tau_r = f_r \frac{\rho_r V_r^2}{8} \tag{31}$$

where the friction factor for fully developed laminar incompressible flow between parallel plates is given by

$$f_r = \frac{96}{Re_r} \quad . \tag{32}$$

With the hydraulic diameter for parallel plates defined as twice the liquid film thickness, the Reynolds number can be expressed as

$$Re_r = \frac{V_r D_h}{\nu} = \frac{2\delta V_r}{\nu} \quad . \tag{33}$$

The wall shear stress then becomes

$$\tau_r = \frac{6\rho\nu V_r}{\delta} \quad . \tag{34}$$

The frictional force can now be expressed as

$$F_f = \frac{6\rho\nu V_r \theta r \Delta r}{\delta} \quad . \tag{35}$$

The forces F_r and $F_{r+\Delta r}$ are simply equal to the product of the local pressure and the appropriate area.

Substituting the expression for the various forces and using Equation (3) in the momentum equation (Equation (25)) yields

$$P_r \theta r \delta + \rho r \theta \delta V_r^2 + 2P_r \Delta r \delta \sin\frac{\theta}{2}$$

$$= \frac{12\rho\nu V_r \theta r \Delta r}{\delta} + (P_r + \Delta P)\theta(r + \Delta r)\delta + \rho\theta\delta(r + \Delta r)(V_r + \Delta V)^2 \quad . \tag{36}$$

Eliminating second order terms, letting sin $\theta/2$ equal $\theta/2$, and solving for ΔP yields

$$\Delta P = \frac{-12\rho\nu V_r \Delta r}{\delta^2} - \frac{\rho V_r^2 \Delta r}{r} - 2\rho V_r \Delta V \quad . \tag{37}$$

Dividing both sides of this equation by Δr and taking the limit as Δr approaches zero produces the following differential equation for the radial pressure gradient in the liquid film:

$$\frac{dP_r}{dr} = \frac{-12\rho\nu V_r}{\delta^2} - \frac{\rho V_r^2}{r} - 2\rho V_r \frac{dV_r}{dr} \quad . \tag{38}$$

From Equation (6), differentiating with respect to r yields

$$\frac{dV_r}{dr} = \frac{\rho_s V_s}{2\rho\delta} = \frac{V_r}{r} \quad . \tag{39}$$

Substituting into Equation (38) and reducing yields

$$\frac{dP_r}{dr} = - \frac{-6\rho_s \nu r V_s}{\delta^3} - \frac{3\rho_s^2 V_s^2 r}{4\rho\delta^2} \quad . \tag{40}$$

Equation (40) can be integrated to obtain the liquid pressure as a function of r. Integration produces

$$P_r = \frac{-3\rho_s \nu V_s r^2}{\delta^3} - \frac{3}{8} \frac{\rho_s^2 V_s^2 r^2}{\rho\delta^2} + C \tag{41}$$

where C is evaluated by using the boundary condition that $P_r = 0$ at $r = r_e$. Thus,

$$C = \frac{3\rho_s \nu V_s r_e^2}{\delta^3} + \frac{3}{8} \frac{\rho_s V_s^2 r_e^2}{\rho\delta^2} \quad . \tag{42}$$

The upward force on the ice can be determined by integrating P_r over the ice surface area, that is,

$$F_u = \int_{\text{Area}} P_r dA = 2\pi \int_0^{r_e} P_r r dr \quad . \tag{43}$$

Integration yields

$$F_u = \left(\frac{-3\rho_s V_s \nu r_e^2}{2\delta^3} - \frac{3}{16} \frac{\rho_s^2 V_s^2 r_e^2}{\rho\delta^2} = C \right) \pi r_e^2 \quad . \tag{44}$$

For a constant downward velocity of the ice, this upward force is of the same magnitude as the known applied downward force. Thus, for a known downward force and heat flux, T, h, δ, V_s, and the pressure distribution can be determined.

2.6 Solution Technique

As seen in Figure 7, an iterative technique is employed in the computer solution by use of the melt velocity to adjust the balance between the downward and upward acting forces on the ice. Certain system physical and geometrical information as well as an initial V_s estimate are required as initial conditions. Equations (19), (21), (24), and (44) are solved in order. Values for the temperature dependent liquid properties (density, kinematic viscosity, and thermal conductivity) used in Equation (44) are updated during each iteration step by use of the recent Equation (19) solution in their respective polynomial expressions. Details of the polynomial formation are found in Appendix A. The ensuing value for F_u from Equation (44) is compared to the known downward force. Unsatisfactory agreement results in a change of the previous value of V_s and subsequent revaluation of the four equations above. Upon compliance with the acceptable error criteria, the average liquid radial velocity and liquid pressure are calculated at specified steps in radial position away from the centerline by use of Equations (6) and (41), respectively.

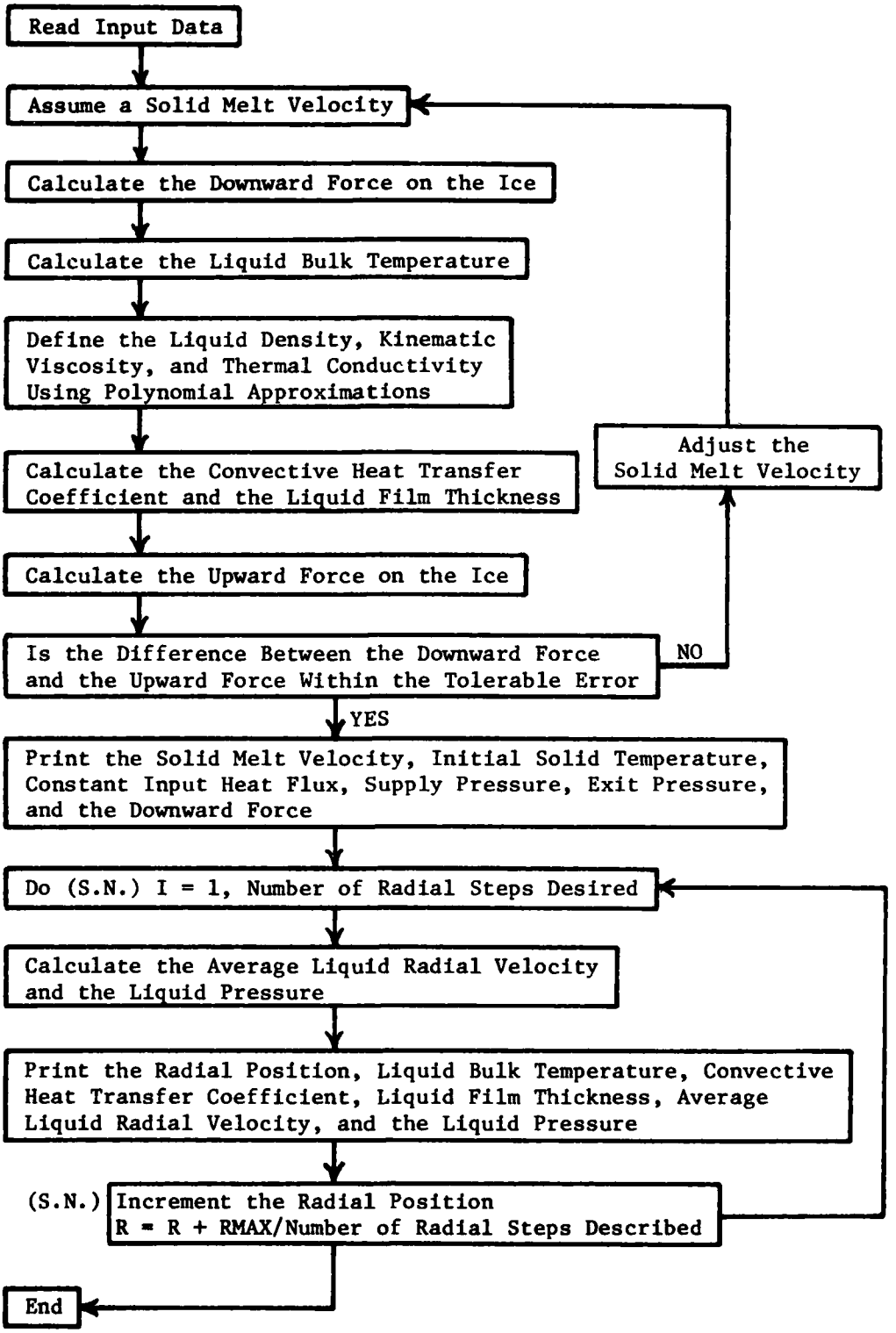

Figure 7. Flow Chart for the Computational Procedure.

CHAPTER III

EXPERIMENTAL INVESTIGATION

3.1 Experimental Concept

The purpose of this experimental investigation was to provide test data for comparison with the analytical model predictions. The test system was designed primarily to create an experimental environment similar to that assumed in the formulation of the analytical model. The reason for this was to create a situation where the test data and the model predictions were directly comparable. The system design tested is not necessarily that which yields the fastest ice melt rates for a given input heat flux and supply pressure.

The complete test facility is shown in Figure 8. A control console, test stand, and data collection system comprise the entire test apparatus. Figure 9 illustrates the overall operating scheme of the test facility. The general method of operation involved forcing the solid test specimen against a heated surface by use of a known supply pressure. The melted fluid left the liquid film region by exiting radially into four collector cans. Ramrod position and various temperature signals were conditioned and recorded as a function of time and provided experimental data for the downward speed of the ice and a temperature history of the heated block and exiting fluid.

3.2 Apparatus

The test specimen assembly shown in Figure 10 is the core of the experimental apparatus. Its basic purpose was to provide a structure

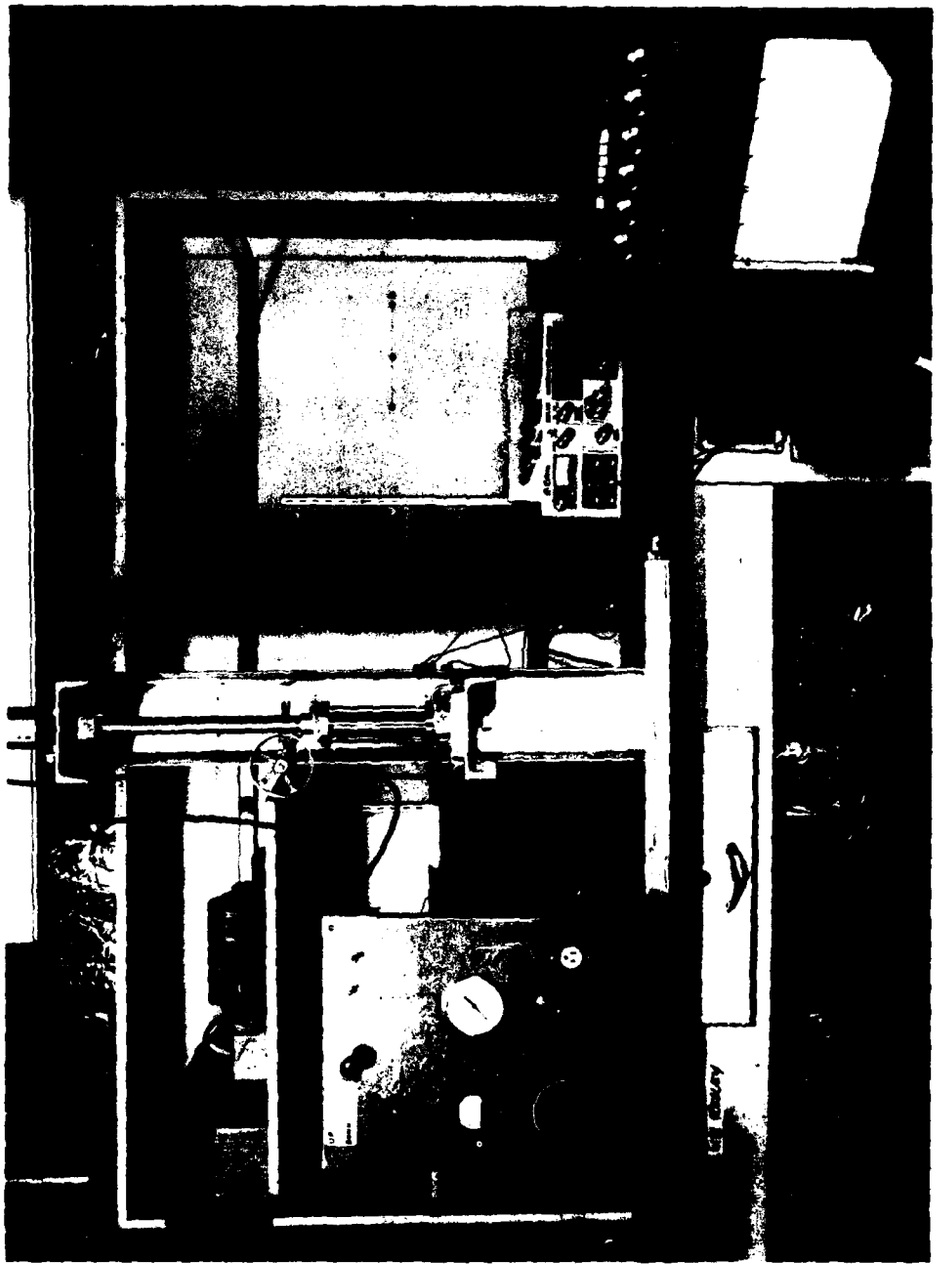

Figure 8. Photograph of the Complete Test Facility.

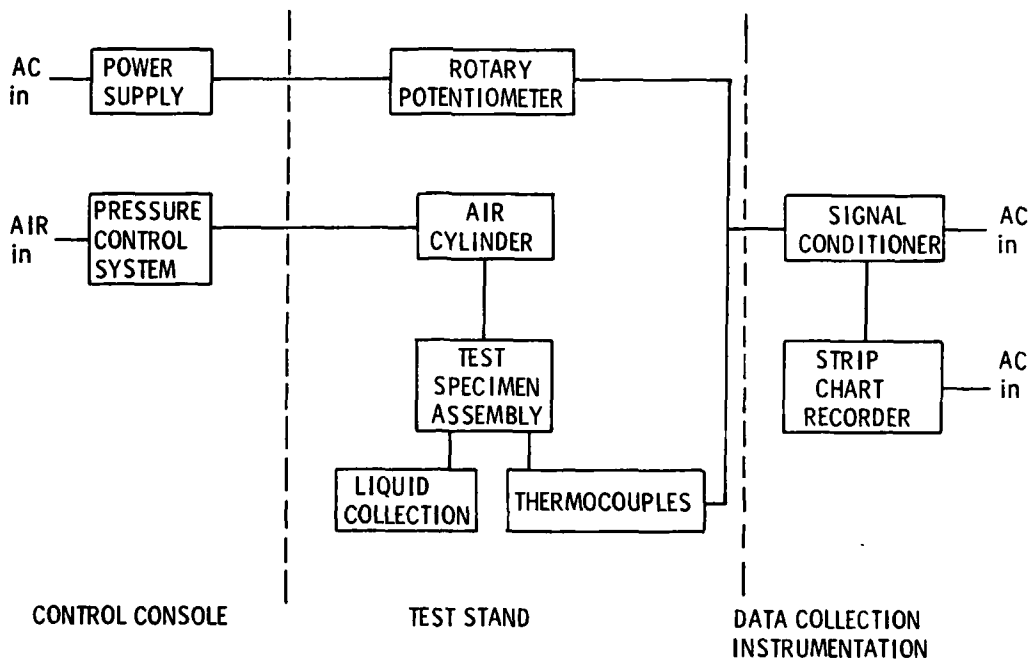

Figure 9. Schematic of the Test Facility.

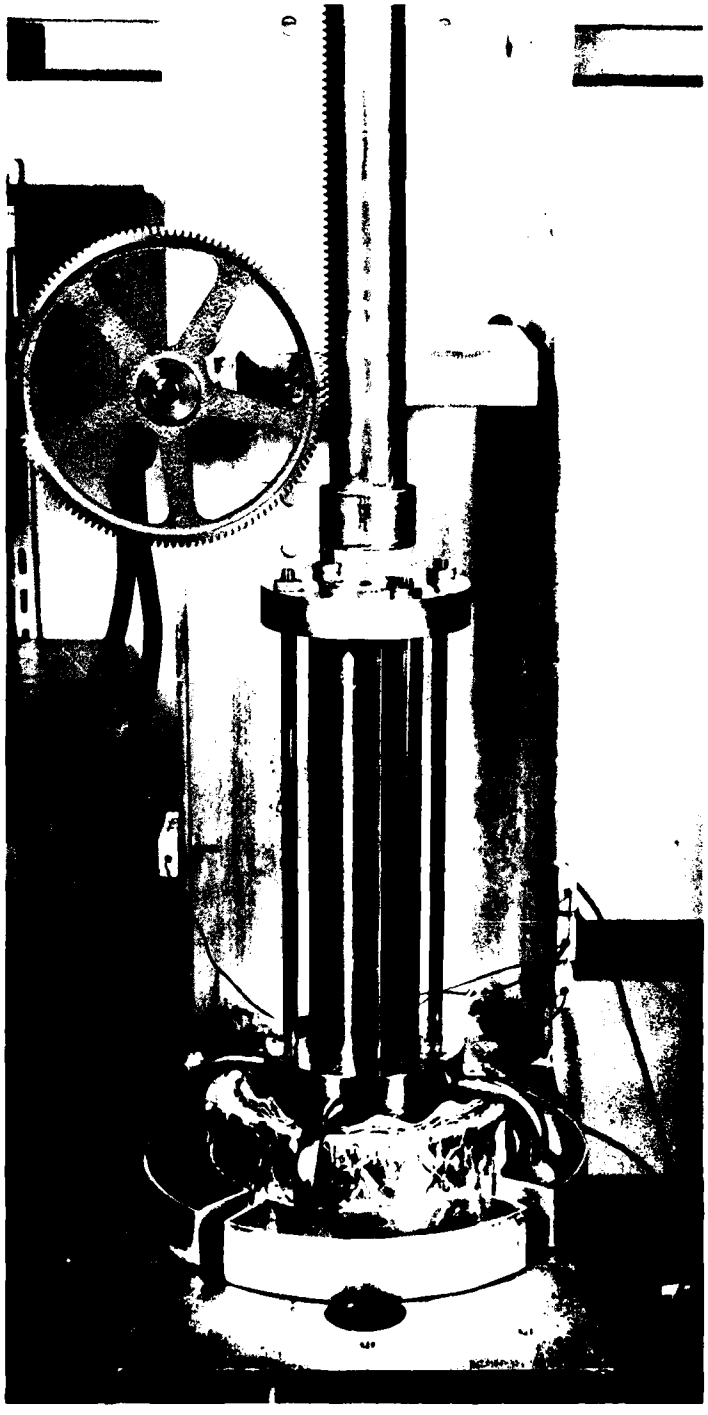

Figure 10. Photograph of the Test Specimen Assembly.

containing the thermal source and solid specimen in such a geometry as to permit radial fluid exit and eventual collection while allowing for the strategic placement of thermocouples for temperature measurement. The figure shows the complete assembly structure in position on the test stand. Foil-backed, hot block insulation can be seen in the center of the figure surrounded by the four aluminum collector cans used to store the exiting fluid. Tie rods secure the test cylinder to the collar piece on the hot block. Attached to the end of the ramrod is a piston which slides into the bore of the test cylinder. The large gear meshes with a rack on the ramrod and is attached to the center post of a rotary potentiometer which measures ram position. Chromel-Alumel thermocouple probes enter the test specimen assembly at various locations. Their connectors are fastened to the test stand in the background. Chromel-Alumel electronic ice point reference junctions are seen in the lower right-hand corner of the figure.

Figure 1 is a cutaway view of the test specimen assembly which identifies the various parts composing the assembly: the hot block, collar, test cylinder, cap, tie rods, elbows, and insulation. The materials used in the construction of the collar and hot block are capable of withstanding temperatures on the order of 426.7°C (800°F) without undergoing any substantial change in physical characteristics. The test cylinder is a standard size of stainless steel tubing machined to fit into a collar milled from a stainless steel rod. Four tabs on the test cylinder end nearest the hot block support the cylinder on the collar piece and provide a clearance gap for liquid passage out of the melt zone. The tab length was sized to be about ten times the expected liquid film thickness in the melt zone to minimize obstruction due to

the test cylinder walls. Steel tie rods attach an aluminum cap on the top of the test cylinder to the collar piece. This containment structure firmly secures the test cylinder to the collar. An aluminum piston was used to uniformly apply the supply pressure to the test specimen in the test cylinder. Leaded copper was used for the hot block material due to its superior thermal conductivity and good machinability. A large diameter copper rod was machined down to exactly match the inside diameter of the test cylinder in the region nearest the melt zone. Insulating paper was cemented to the hot block's outer surface by use of a ceramic paste. A layer of 6.35 mm (0.25 in) foil-backed insulating blanket was wrapped around the insulating paper. These insulating layers diminished the heat loss from the block.

An important design criteria for the test assembly was the requirement of assuring unobstructed liquid radial flow exiting from the melt zone. Figure 11 is a photograph of the assembled hot block and collar. The hot block material seen in the center of the structure has the same diameter as the solid test specimen. A smooth transition from the hot block surface to the collar face was provided by careful assembly of the collar and hot block and by use of varying thicknesses of insulation between the two pieces. This procedure minimized flow obstruction. The liquid flowed through a recess in the collar, past a thermocouple probe in the exit port, and then into the collector cans. An O-ring seal between the collar and the test cylinder sealed this portion of the liquid circuit. The thermocouples in the collar were sealed with SILASTIC 732, a silicon compound.

Distilled water was used to form the test specimens to insure known water properties. The pressure acting on the cylinder was regulated to

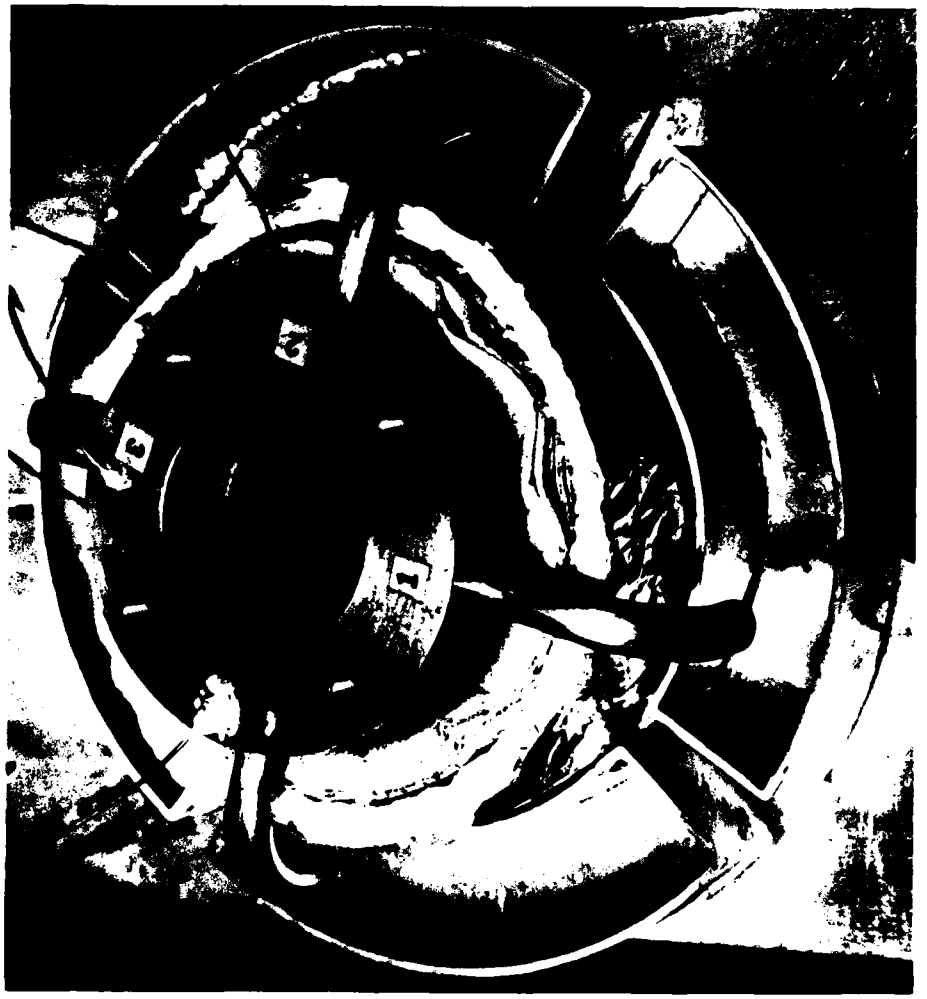

Figure 11. Photograph of the Assembled Hot Block and Collar.

produce a controlled, constant force on the test sample. As discussed, the geometry of the test cylinder end, collar, and hot block were chosen to produce radial flows with minimum restriction. The order of magnitude difference in the thermal conductivities of the leaded copper and stainless steel, coupled with the insulation, promote approximately one-dimensional heat transfer along the copper block axis. Also, the geometry of the hot block is such that the difference in diameters between the section near the melt zone and the remainder of the block acts to funnel the heat flow from the large diameter section into the smaller section. This limits the radial heat transfer effects in the smaller section.

The test stand seen in the center of Figure 8 was constructed from several sections of aluminum channel welded together. Atop the stand is an air cylinder capable of handling 1.724 MPa (250 psia) at its inlet ports. The cylinder is the double acting style which allows the same pressure source used to extend the ramrod to also be used to retract it. A guide bar and rod addition extend from the region near the top of the stand to the upper platform. The guide bar assists in directing the ramrod linearly against the ice specimen in the test cylinder. The rod extension is brass and has a rack soldered into it that meshes with a gear attached to a rotary potentiometer. The potentiometer is then used to indicate the ramrod position. The lower platform on the test stand forms the base for the test specimen assembly. The assembly is bolted to an adapter plate which is in turn bolted to the platform. Four collector cans sit on the platform beneath their respective liquid exit elbows. The region below the lower platform is left open to permit the use of a propane torch in heating the hot block.

The control console has some hardware not used in the present study. Only those items used will be mentioned. The only function of the control console was to control the supply pressure magnitude and direction of application. Compressed air was selected for use in the pressure control system and for operating the double acting cylinder since there was convenient access to an air compressor. Figure 12 is a schematic of the pressure control system. The system is capable of handling pressures up to 1.379 MPa (200 psig).

The magnitude of the source pressure is controlled with a pressure regulator. A gauge is used to monitor the pressure level to the air cylinder. Calibration of the actual force applied to the test specimen in terms of the regulator pressure was done by placing a force transducer under the ramrod and applying selected pressures to the cylinder. Since the test specimen area over which the ramrod force acts was known, the pressure at the heated surface was then determined in terms of the regulator pressure. Figure 13 shows the resulting data.

The direction of application of the regulator pressure is selected by using two hand valves and two solenoid valves. The regulator pressure can be directed to cause the ramrod to either extend or retract. Ramrod control is illustrated with the aid of Figure 12. With hand valve No. 1 open and hand valve No. 2 closed, the toggle switch can be thrown to the extend position which closes solenoid valve No. 1 and opens solenoid valve No. 2. This directs air pressure to the top port of the air cylinder and provides a venting system through which the gas below the cylinder's piston can escape. The opposite procedures are applied to retract the ramrod.

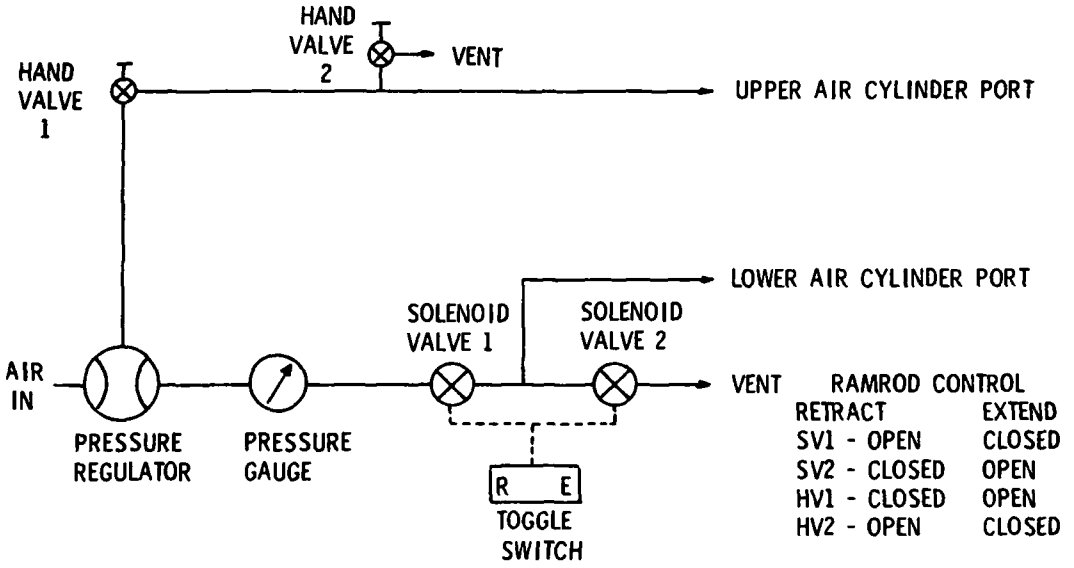

Figure 12. Schematic of the Pressure Control System.

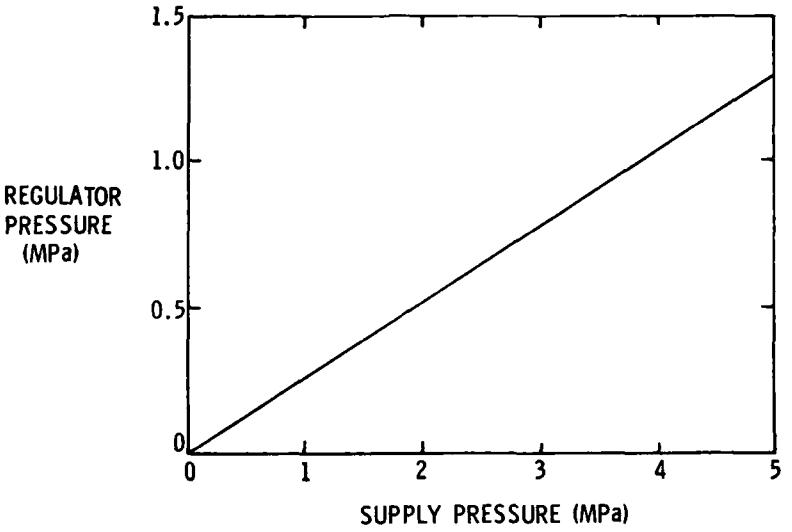

Figure 13. Supply Pressure Calibration Curve.

3.3 Instrumentation

The instrumentation system for the test facility provided data collection for the ramrod position and various temperatures as a function of time. Figure 14 shows schematically the items comprising the instrumentation system. Small grounded Chromel-Alumel thermocouples 0.79 mm (0.031 in) in diameter were used to sense the temperature of the liquid as it passed through two of the four outlet ports in the collar piece of the test specimen assembly. Two additional thermocouples of the same type placed a known axial distance apart sensed the temperature on the centerline of the hot block. They were located in the reduced diameter portion of the block near the hot block/liquid interface. The size and type of thermocouple selected were chosen to promote placement accuracy and yet remain sturdy enough for installation with standard techniques. The thermocouples were electronically referenced to $0^{o}C$ and then amplified in the signal conditioning unit to provide 5 V DC outputs for the desired full scale temperature level. This output voltage was then recorded and displayed on a Brush strip chart recorder as a function of time. The rotary potentiometer was used to sense the ramrod position. Its output was conditioned and recorded on the strip chart and therefore provided the data required to calculate the solid melt velocity.

The small size and grounded thermocouple style produced good time response to a step increase in temperature and minimized the level of flow disturbance in the exit ports. A time constant of 1.9 sec was specified by the manufacturer (21). This response is nearly twice as fast as an ungrounded style thermocouple of the same size. Figure 15 illustrates the thermocouple placement in the test specimen assembly. As seen in the figure, the thermocouples sensing the fluid temperature

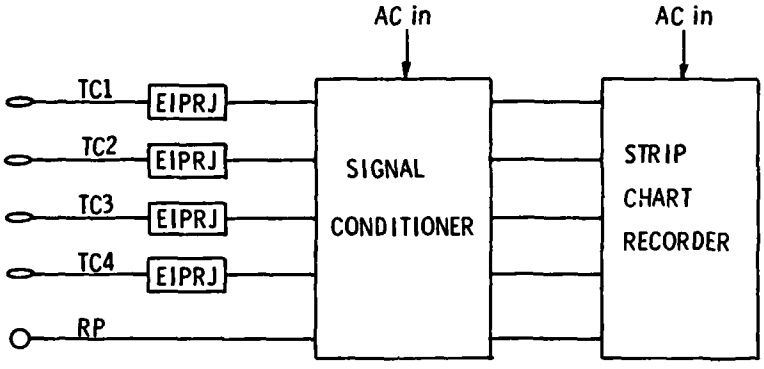

TC – THERMOCOUPLE

EIPRJ – ELECTRONIC ICE POINT REFERENCE JUNCTION

RP – ROTARY POTENTIOMETER

Figure 14. Schematic of the Instrumentation System.

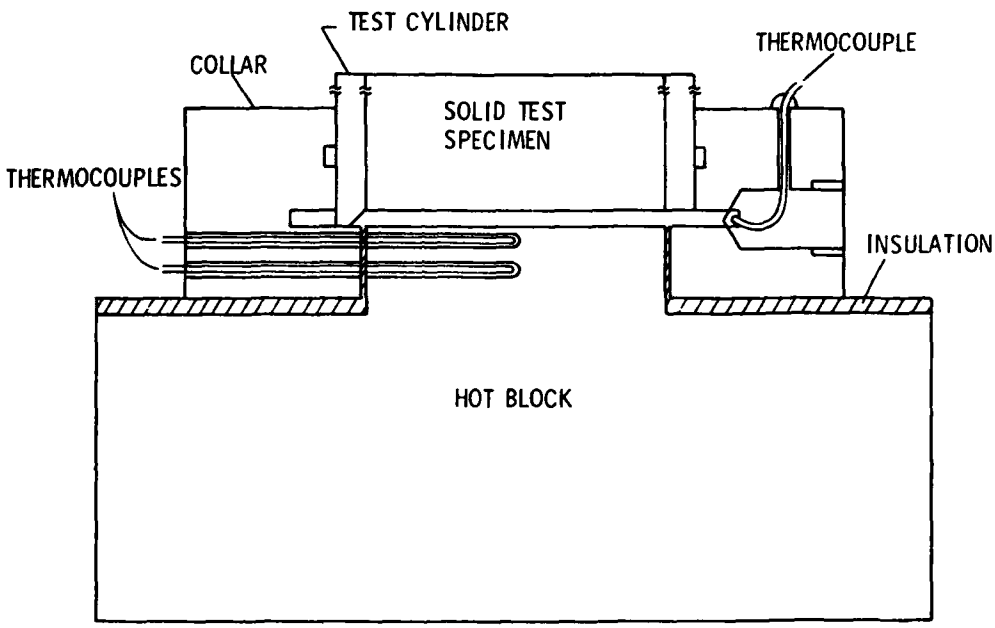

Figure 15. Thermocouple Placement.

are for the most part located in the outlet ports of the collar. Only the tip of the probe approaches the relatively small annular collecting space in the collar. Because the percentage of volume occupied by the probe in the exit port is small, minimal obstruction to the liquid flow in the port occurs. The thermocouples placed in the center of the hot block have approximately 50.8 μm (0.002 in) clearance on the diameter of the hole in the block.

The temperature measuring instrumentation was calibrated by use of an Ectron thermocouple simulator. Figure 16 illustrates schematically how the unit interfaces with the temperature measuring system. This device electronically generates the low level voltage representative of a selected thermocouple type at some selected temperature referenced to a known temperature. Various simulated temperatures were then selected and provided known temperature levels. The zero offset and sensitivity of the strip chart recorder were then adjusted to give the desired full scale temperature range for each temperature signal. By knowing the stroke length of the cylinder, the ramrod position was calibrated on the strip chart. The appropriate recorder channel was adjusted to indicate the known travel length in conveniently read increments of the chart.

3.4 Test Procedure

A test specimen was required for each experiment. To form one, an aluminum piston was assembled into the top end of the test cylinder and the clearance space was sealed with modeling clay. The cylinder was then inverted and distilled water was added. The cylinder was placed in a freezer and allowed to soak for at least 12 hr. For the tests performed in this study, the freezer temperature was -17.8°C (0°F).

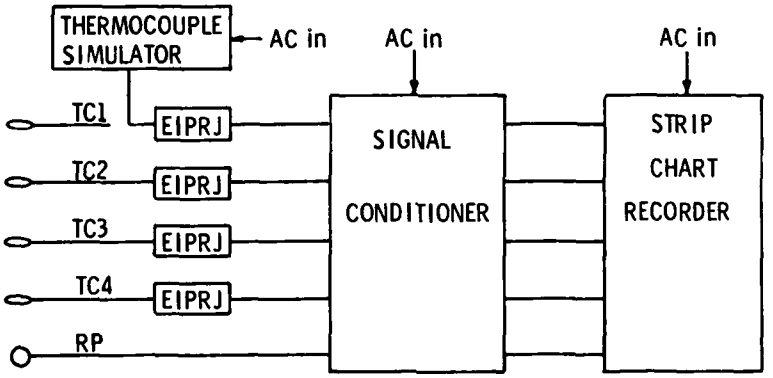

TC – THERMOCOUPLE

EIPRJ – ELECTRONIC ICE POINT REFERENCE JUNCTION

RP – ROTARY POTENTIOMETER

Figure 16. Schematic of the Temperature Measurement Calibration.

Three test cylinders were used for each testing period. Because only one cylinder could be used at a time, the cylinders were insulated and stored in a Styrofoam ice chest containing about 0.91 kg (2 lbm) of dry ice. The required storage time was normally no more than 90 min, and it was assumed that during this time the samples remained at about $-17.8^{o}C$.

All of the electronics in the test facility were given adequate time to warm up and stabilize prior to system calibration and subsequent testing. This time period was never less than 30 min. Calibration of temperature and rod position sensors was then performed as previously described. The full scale ranges for the information recorded is shown in Table 1.

Of the possible melt energy sources considered, a concept using stored heat energy in a copper block was felt to be the best. This was done because steady state heating required prohibitive source temperatures for the thinnest copper blocks that were structurally feasible. Transient cooling of the block offered an acceptable means of achieving the desired melting rates. The solid melt velocities targeted for this study were on the order of 1.27 cm/sec (0.5 in/sec). Storage of the thermal energy in a hot block prior to forcing the test specimen against the block surface rendered the heat rate to the test specimen independent of the initial energy source and tied it to the thermal properties of the block. The resulting melt velocity had an approximately linear profile over relatively large segments of a given test run. The preheat temperature of the hot block was found to have a direct influence on the melt velocities associated with a given supply pressure. Hot block preheat temperatures from $65.6^{o}C$ ($150^{o}F$) to $260^{o}C$ ($500^{o}F$) were used in the

Table 1. Recorded Test Data.

ITEM	RANGE
RAMROD POSITION	0 to 25.4 cm
HOT BLOCK TEMPERATURE 1 (NEAREST LIQUID/SOLID INTERFACE)	0 to 65.6^{o}C
HCT BLOCK TEMPERATURE 2	0 to 121.1^{o}C
LIQUID BULK TEMPERATURE 1	-6.7 to 48.9^{o}C
LIQUID BULK TEMPERATURE 2	-6.7 to 48.9^{o}C

tests. At any supply pressure tested, the higher preheat temperature yielded higher melt velocities at each stage of a run.

The test cylinder was assembled to the test stand after the hot block preheating had been completed. This was done to minimize the time the test specimen was exposed to heat conduction losses from the copper block. The test cylinder was fastened securely to the test stand by use of the tie rods and cap. The cylinder walls were heated briefly with the propane torch to free the sample from the cylinder wall. The ramrod was then positioned into the piston in the top of the test cylinder and the data recorder started. The supply pressure level and direction of application were checked and the test was conducted. For the duration of the run, which was anywhere from 3 sec to 1 min, visual observations were made regarding the nature of the liquid flow out of the exit ports. For some tests, the flow was unsteady and randomly selective with regard to which ports it passed through.

The test data obtained were repeatable and consistent. Certain performance anomalies did occur in some of the tests, most notably in the set of test runs at the lowest supply pressure. These anomalies are described in detail in Chapter IV.

Based on the published accuracy of the thermocouples (21) and when the measurement and calibration techniques used are considered, the total data collection system is estimated to have an accuracy of ±5%, that is, the data recorded on the strip chart is estimated to be within 5% of a known input value.

CHAPTER IV

RESULTS AND DISCUSSION

4.1 Experimental Results

The effects of varying supply pressures and input heat fluxes on the ice melt velocity and liquid bulk temperature were investigated through the tests conducted in this study. Whereas the magnitude of the supply pressure was easily controlled, the management of the input heat flux was somewhat indirect. Thermal energy stored in the copper block provided the heat flux. For a given supply pressure, a direct relationship exists between the initial bulk temperature of the hot block and the heat flux leaving the block during a test.

Table 2 illustrates the test matrix followed in this investigation. Although the higher input heat fluxes were of the greater interest since they were expected to yield the higher ice melt velocities, lower values were also tested to produce a more complete picture of the ice melting phenomenon. A minimum of three different supply pressures was selected to illustrate the effect of this variable on the ice melt velocity.

The ice position, two copper block temperatures, and two liquid bulk temperatures were recorded on the strip chart providing test data. These variables were then identified over a selected steady state segment of the test where the ice position and copper block temperature traces exhibited essentially steady behavior. This information, the supply pressure, initial copper temperature, and initial ice specimen temperature were then tabulated and provided a listing of all the raw

Table 2. Experimental Test Matrix.

INITIAL HOT BLOCK TEMPERATURE (^{o}C)	SUPPLY PRESSURE (MPa)		
	1.269	2.592	3.606
65.6	X	X	X
93.3	X	X	X
121.1	X	X	X
148.9	X	X	X
171.1	X	X	X
193.3	X	X	X
215.6	X	X	X
237.8	X	X	X
260.0	X	X	X

test data. Tables B-1, B-2, and B-3 in Appendix B contain the raw data obtained for the tests conducted at the supply pressures of 1.269 MPa (184 psig), 2.592 MPa (376 psig), and 3.606 MPa (523 psig), respectively. Elapsed time for complete melting of the nominal 15.24 cm (6 in) length test specimen ranged between 3.3 and 54 sec. It is noted that some melting of the ice occurs during assembly of the test cylinder to the test stand. Therefore, the time limits mentioned cannot be extrapolated to estimate the ice melt velocity. These extremes in test duration only indicate over what kind of time span a steady state portion of data could be extracted.

The raw data was then reduced to a more useful form. The ice melt velocity during a specified time interval was determined by use of the available ice specimen position information in the equation below:

$$V_s = \frac{z(t_2) - z(t_1)}{t_2 - t_1} \quad . \tag{45}$$

The temperature difference in the hot block was found by subtracting the block temperature closer to the liquid film T_c from the block temperature T_h farther away from the block/liquid interface. This temperature difference was as small as 1.7°C (3°F) and as large as 43.9°C (79°F) for the experiments conducted and nearly constant over the selected data time intervals. The input heat flux to the system as measured in the hot block was then determined by use of the conduction heat transfer equation:

$$\dot{Q}''_k = \frac{k(\Delta T)}{\Delta z} \quad . \tag{46}$$

The thermocouple spacing in the hot block Δz was measured to be 2.972 mm (0.117 in) ±0.254 mm (0.01 in). The thermal conductivity of the leaded copper used in the calculation was 385.9 W/m-^{o}C (223 Btu/hr-ft-^{o}F) [22]. Another method for estimating the input heat flux was used as a cross-check. Solving Equation (19) for the heat flux results in the following expression:

$$\dot{Q}''_t = \rho_s V_s \left(C_p (T - T_m) + h_{sf} + C_{ps}(T_m - T_s)\right) \quad . \tag{47}$$

This equation is obtained from the first law analysis on the liquid film and provides a way of determining the total heat flux into the system required to melt the ice at some constant velocity V_s. Tables 3, 4, and 5 list the results of reducing the raw data by use of Equations (45), (46), and (47) for the three supply pressures. Figures 17 and 18 are plots of the ice melt velocity versus $\dot{Q}''_k$ and $\dot{Q}''_t$, respectively. When it is assumed that all of the available energy was used to melt the ice and none was used to raise the liquid temperature, the maximum rate line in the figures identifies the maximum ice melt velocity possible for a given input heat flux. Letting $\dot{Q}''_t$ equal $\dot{Q}''_m$ and solving Equation (18) for V_s yields

$$V_{s_{max}} = \frac{\dot{Q}''_i}{\rho_s \left(C_{ps}(T_m - T_s) + h_{sf}\right)} \quad . \tag{48}$$

This equation defines the maximum melt rate line. Figures 19 and 20 show the liquid bulk temperature as a function of $\dot{Q}''_k$ and $\dot{Q}''_t$, respectively. The solid lines in the four figures indicate a least squares approximation to the data. The standard error of estimate on the

Table 3. Reduced Data, P_s = 1.269 MPa.

RUN NUMBER	V_s (mm/sec)	T (^{0}C)	$\dot{Q}''_k$ (MW/m^2)	$\dot{Q}'''_t$ (MW/m^2)	LOCATION RELATIVE TO ANOMALY
52	8.26	38.3	3.753	3.971	N
53A	3.15	12.2	1.299	1.202	N
53B	2.92	11.7	1.154	1.110	N
54	5.87	22.2	2.596	2.463	N
55	9.22	41.1	4.113	4.535	N
56A	8.86	23.3	2.741	3.763	A
56B	10.08	12.2	3.104	3.851	A
57A	2.92	18.9	1.082	1.192	N
57B	2.26	12.2	0.795	0.864	N
58	7.09	33.9	3.104	3.293	N
59A	7.06	38.3	3.104	3.397	B
59B	8.15	23.3	2.451	3.457	A
60	4.85	24.4	2.164	2.078	N
61	5.56	29.4	2.668	2.489	N
62	8.20	36.1	3.678	3.876	N
63	7.09	33.9	3.249	3.293	N

B – BEFORE ANOMALY A – AFTER ANOMALY N – NO ANOMALY PRESENT

Table 4. Reduced Data, P_s = 2.592 MPa.

RUN NUMBER	V_s (mm/sec)	T (^oC)	$\dot{Q}''_k$ (MW/m^2)	$\dot{Q}''_t$ (MW/m^2)	LOCATION RELATIVE TO ANOMALY
37	6.86	7.8	2.236	2.504	N
38	6.35	7.8	2.164	2.318	A
39A	3.86	8.9	1.299	1.426	N
39B	3.15	4.4	0.937	1.110	N
40	14.94	12.8	5.267	5.734	A
41A	6.35	9.4	2.164	2.359	A
41B	6.15	7.2	1.877	2.230	A
42A	2.69	5.0	0.577	0.956	A
42B	1.35	4.4	0.214	0.473	A
44	13.79	10.0	4.617	5.150	A
45	11.05	5.0	3.391	3.914	A
46	12.45	11.1	4.327	4.696	A
47A	8.56	27.2	3.678	3.753	B
47B	11.53	14.4	3.823	4.501	A
48	9.19	7.2	2.668	3.337	A
49	14.50	10.6	4.832	5.444	A
50A	12.22	18.9	4.258	5.072	A
50B	14.12	12.2	4.472	5.390	A
51	12.85	12.2	4.617	4.908	A

B – BEFORE ANOMALY A – AFTER ANOMALY N – NO ANOMALY PRESENT

Table 5. Reduced Data, P_s = 3.606 MPa.

RUN NUMBER	V_s (mm/sec)	T (^oC)	$\dot{Q}''_k$ (MW/m^2)	$\dot{Q}''_t$ (MW/m^2)	LOCATION RELATIVE TO ANOMALY
64	12.90	15.6	4.617	5.091	A
65A	5.51	10.0	1.659	2.059	A
65B	4.04	8.3	1.372	1.482	A
66A	6.93	32.2	3.031	3.176	B
66B	9.29	10.6	3.031	3.491	A
67	15.24	13.9	5.554	5.914	A
68A	7.85	26.7	2.668	3.428	B
68B	7.95	10.0	2.668	2.968	A
69A	4.37	5.6	1.372	1.558	A
69B	3.12	5.6	1.009	1.113	A
70	14.94	10.0	5.339	5.576	A
71	13.74	11.7	4.113	5.219	A
72	10.82	12.2	3.536	4.125	A
73	14.38	15.0	5.122	5.639	A
74	10.41	10.6	3.173	3.813	A
75	13.51	11.1	4.472	5.103	A

B – BEFORE ANOMALY A – AFTER ANOMALY N – NO ANOMALY PRESENT

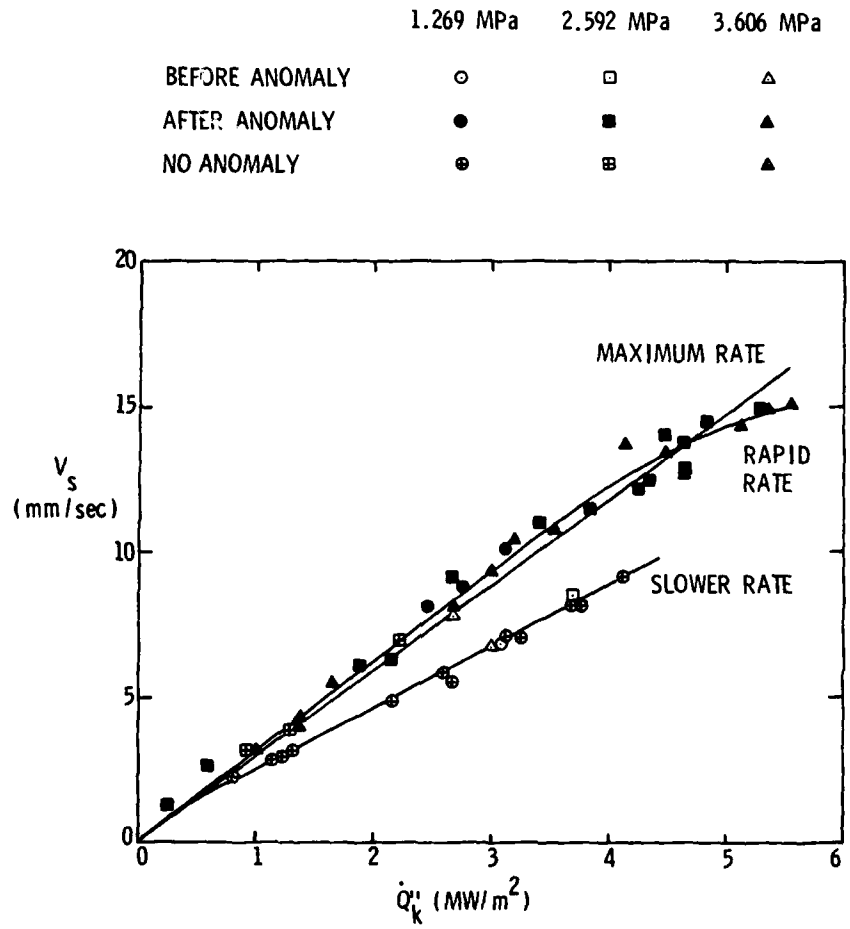

Figure 17. Experimental Results, V_s versus $\dot{Q}''_k$.

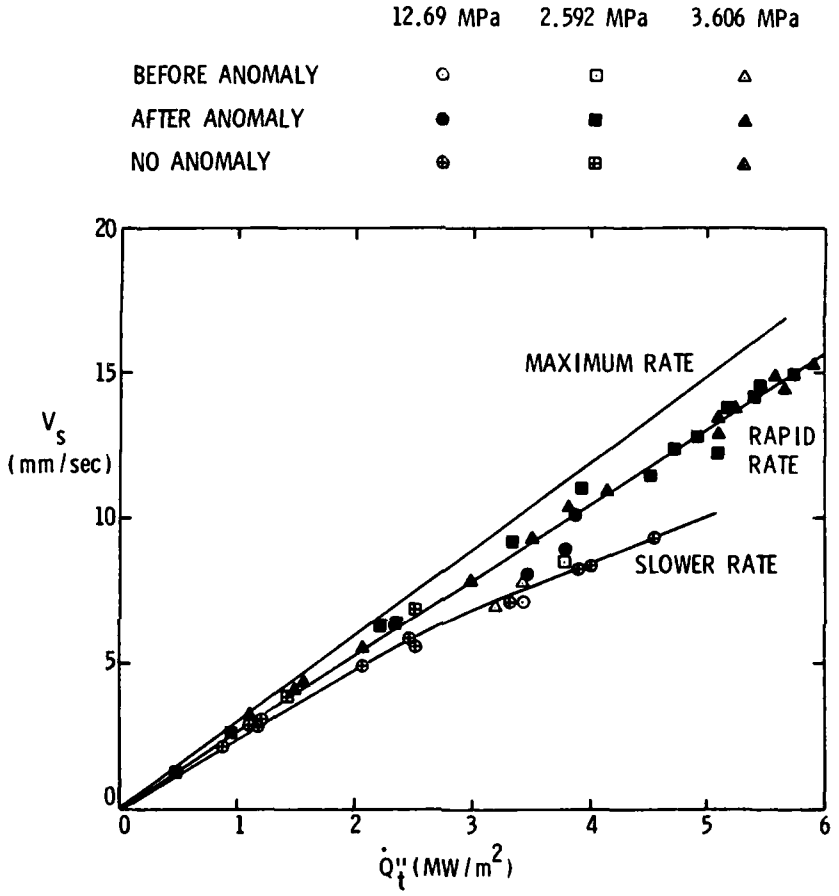

Figure 18. Experimental Results, V_s versus $\dot{Q}''_t$.

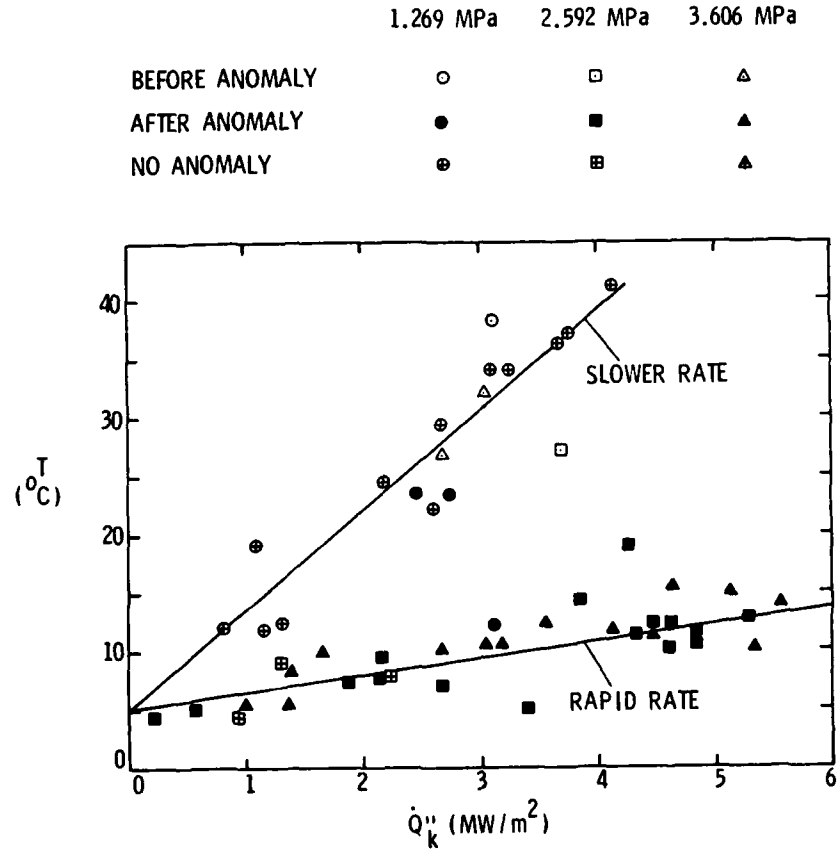

Figure 19. Experimental Results, T versus $\dot{Q}''_k$.

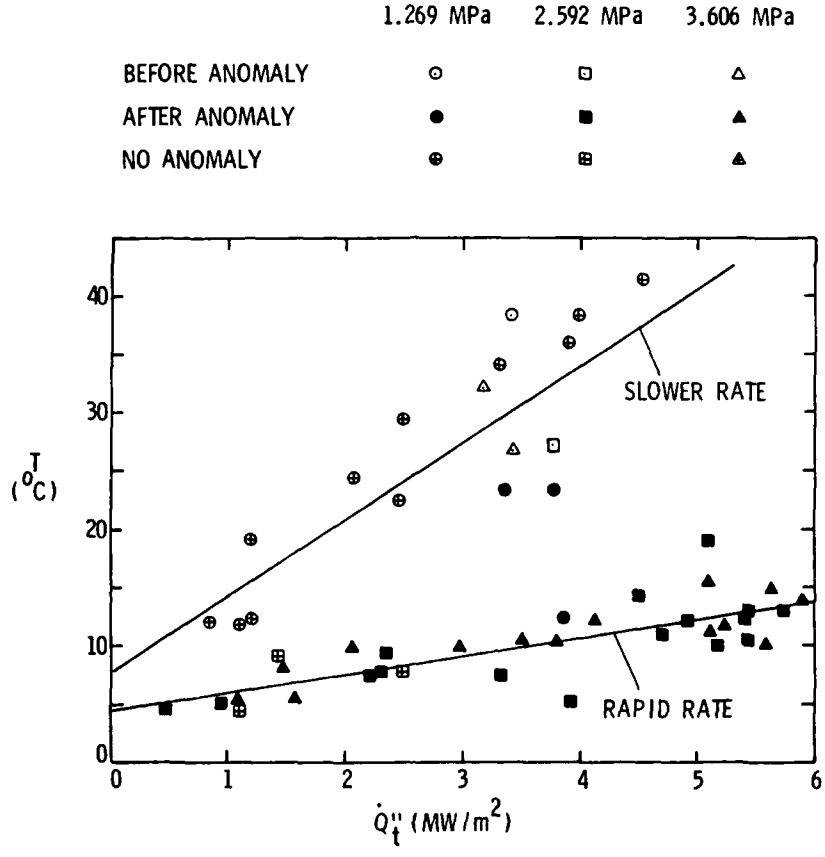

Figure 20. Experimental Results, T versus $\dot{Q}''_t$.

velocity in Figures 17 and 18 is about 0.325 mm/sec (0.0128 in/sec), and the maximum absolute error is approximately 0.851 mm/sec (0.0335 in/sec). For Figures 19 and 20, the standard error of estimate on the liquid bulk temperature is nearly 3.4°C (6.08°F), and the maximum absolute error is about 8°C (14.48°F).

In general, Figure 17 shows the ice melt velocity increasing as the input heat flux measured in the hot block increases. Further inspection of the figure discloses that there appears to be two distinct curves describing the relationship. All of the data points for the supply pressures of 2.592 MPa and 3.606 MPa lie along the curve having the greater slope; only two data points fall on the more shallow curve. The nature of the data scatter for these two supply pressures indicates that the supply pressure has very little apparent influence on the ice melt velocity for a given input heat flux. The majority of the 1,269 MPa data, on the other hand, lie along the lower curve with three data points closely following the steeper curve. Close examination of the strip chart records, particularly the ice position and hot block temperature traces, revealed that sudden changes in ice position and hot block temperatures occurred during most test runs, normally in the first half of the run time. In many instances, the changes were very abrupt. Some unknown event must occur in the test system which creates these anomalies. As noted in Tables 3, 4, and 5, the reduced data for each test are labeled to indicate the relative position of the data segment with respect to the irregularities. In checking the location of the data points in Figure 17 for all three supply pressures, it was found that all data obtained prior to the anomaly fell along the slower rate curve and data obtained after an anomaly fell along the rapid rate

curve. That data obtained from tests having no anomalous behavior fell along the slower rate curve for low pressure tests and along the rapid rate curve for the other two pressures.

Figure 19 illustrates the two regime behavior also in the relationship between the liquid bulk temperature and the input heat flux measured in the hot block. There is greater data scatter in this figure than in Figure 17, which reflects the uncertainty associated with interpreting the rather unsteady liquid bulk temperature as recorded on the strip chart. Again, the higher supply pressure data tend to follow one curve and the lower pressure test data follow the other.

The slower rate curves in Figures 17 through 20 demonstrate degraded melting performance and represent a melting phenomenon different from that modeled. The nature of the mechanism producing the anomaly has not been determined absolutely by use of the test data. The hot block temperature and ramrod position information recorded on the strip chart does, however, provide some insight as to what the mechanism may be. As mentioned previously, the change occurred suddenly and rather violently. Normally, an instantaneous change in rod position on the order of 5.08 mm (0.2 in) occurred followed immediately by a very rapid decay of the previously steady hot block temperatures. This sudden movement of ice and subsequent drop in block temperature could indicate the presence of a liquid cavity in the center of the ice sample. Figure 21 illustrates this concept. This configuration is hydrodynamically stable. The necessary heat transfer, on the other hand, is more difficult to explain.

At steady state conditions with the ice specimen moving downward at some velocity, the heat transfer rate measured at the hot block

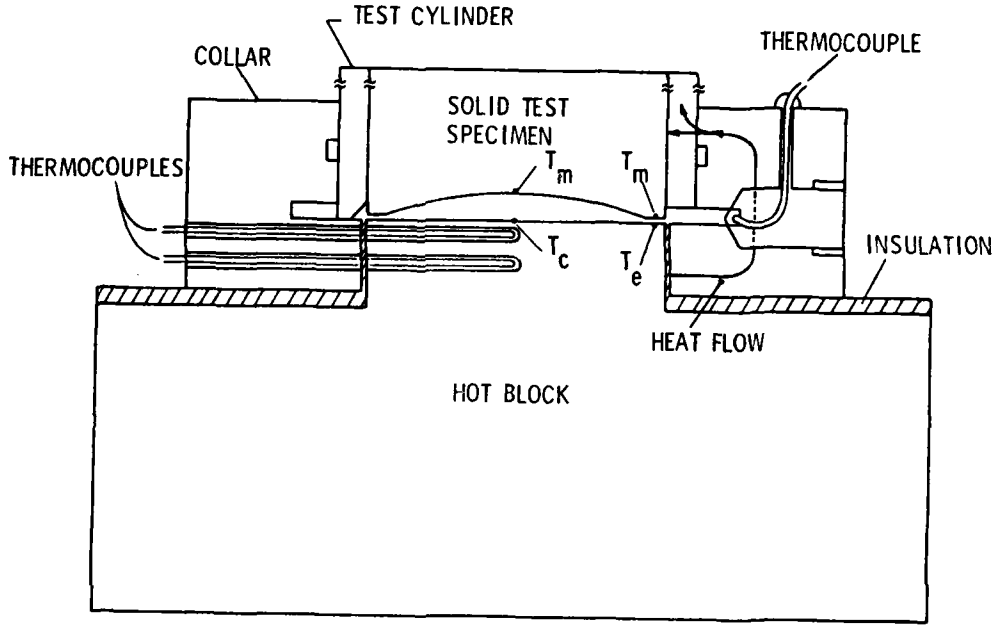

Figure 21. Thermocouple Placement and Cavity Concept.

centerline must be the same as that measured at the exit radius. When the liquid flow is considered to be laminar, the heat transfer rates to the ice are simply expressed as conduction process which yield

$$\dot{Q}''_i = \frac{k(T_c - T_m)}{\delta_c} = \frac{k(T_e - T_m)}{\delta_e} \quad . \tag{49}$$

Since δ_c is much greater than δ_e, the temperature difference across the film at the centerline $(T_c - T_m)$ must then be greater than the temperature difference at the exit radius $(T_e - T_m)$ for the ratios to remain equal. This then means that the centerline temperature of the hot block at its free surface must be greater than the temperature measured at the exit radius and therefore the existence of radial outward heat transfer is indicated. This heat transfer condition is known to exist prior to the initiation of a test. This is true because the energy transfer takes place through the collar and into the cold test cylinder walls during the time required to assemble the test cylinder retaining structure to the test stand (see Figure 21). A significant portion of the test specimen is melted during the 1 to 2 min needed to secure the assembly.

The cavity concept is further supported by visual observations made on several ice samples that were removed from their test cylinders. Test hardware design precluded observation of the liquid film during a test. Examination of the samples revealed that the significant quantities of entrapped air are found near the centerline of the specimens for the full length of the sample. The fact that the air seemed to collect near the cylinder centerline during freezing means that there is a radial distribution of apparent ice density in the sample, with the

apparent density being the lowest at the centerline and increasing as the clear ice is approached at the exit radius. If equal heat transfer rates are applied at the cylinder's centerline and exit radius, it can be shown that the liquid temperature at the centerline must be higher than at the exit radius for equal ice velocities; hence, the film thickness must be greater to get the same input heat transfer rates from the hot block. The porosity of the ice due to the air also provides paths for melted solid to pursue. Under the influence of the high pressures predicted near the centerline, the flow of liquid into the porous zone could be a significant contributor to the creation and growth of the cavity.

Conceptually, the sudden ramrod position change is caused by the combined effects of the applied downward force on the ice and the growth of the liquid cavity. The cavity grows axially and radially and therefore erodes away the amount of ice near the exit radius. Eventually the ice near the exit radius can no longer support its share of the downward force and fractures. This allows the liquid in the cavity to quickly be expelled and brings the centerline ice into near contact with the hot block; thus, the block's surface temperature is suddenly lowered. The same result could be obtained if the liquid in the cavity encountered a fracture in the ice and weakened it until a sudden break occurred. As the hot block temperature T_c decreases toward T_e, a more uniform block surface temperature distribution exists. At some point in time, the relationship between the bulk copper temperature near the melt zone and the bulk collar temperature changes and favors a radial inward transfer of heat. This inward heat flow is never well established, however, because of the large difference in thermal conductivity between

the copper hot block and the stainless steel collar (20.76 W/m-^{o}C versus 385.8 W/m-^{o}C). The more significant heat flow into the instrumented portion of the hot block would now be transferred axially from the thermal energy stored in the large copper mass below. The cavity, therefore, once removed would probably not return.

Since they are only estimates of the conduction heat transfer in the hot block, values of $\dot{Q}''_k$ may be thought of as minimum input heat fluxes. Although the heat transfer from the block to the liquid was assumed to be one-dimensional, it is not certain that additional routes for transferring energy into the ice are not available. Inspection of Figure 17 supports this hypothesis. This indicates conditions where the measured ice melt velocity for a corresponding calculated input heat flux exceeds the largest possible value. Care in the design of the test specimen assembly was taken to minimize the influence of the secondary heat transfer paths, but their presence cannot totally be eliminated. Heat transfer from the collar piece through the test cylinder walls into the ice specimen is the most obvious contributor.

Values for $\dot{Q}''_t$, on the other hand, are based on conservation of energy and are calculated by use of a measured ice melt velocity and liquid bulk temperature. These values are estimates of the total heat transfer supplied to the ice specimen through all paths. The ice melt velocity measurement can be considered to be rather accurate; the measurement of the liquid bulk temperature, however, is subject to three error sources.

The first source of error is the ±5% level mentioned earlier which describes an estimation of the total accuracy of the temperature measuring instrumentation when one accounts for thermocouple

characteristics, temperature calibration procedures, etc. A second source of error is introduced because of the irregularity of the liquid bulk temperature traces on the strip chart. Assignment of an average value to these temperatures was done subjectively. The final error source is a result of the placement of the thermocouple sensing the liquid bulk temperature. These probes do not exactly measure the fluid temperature at the edge of the liquid film as it exits the melt zone. The tip of the probes approach the recess space in the collar piece and all of the probe sheath is exposed to liquid flow in the exit ports. Figure 15 illustrates the thermocouple location. Fluid exiting the melt zone and collecting in the collar piece prior to measurement has the opportunity to possibly increase in temperature via heat transfer from the collar. As the fluid passes the probe tip, the liquid may be at a somewhat higher temperature than that truly characteristic of the liquid film exit flow. Also, heat transfer between the collar and the probe sheath and between the liquid present in the ports and the probe sheath would tend to influence the thermocouple junction at the probe tip and possibly create a higher temperature level than that actual exit flow temperature.

If the liquid bulk temperature measurements were totally accurate and the assumed ice density and specific heat values were reasonable, the $\dot{Q}''_t$ estimation of the input heat flux would be a reasonably accurate indication of the actual heat flux. Because of these uncertainties, however, this method of calculating the input heat flux should only be considered to give approximate values.

4.2 Analytical Results

Results using the analytical model described in Chapter II were obtained for the same supply pressures and range of input heat fluxes tested experimentally. The values for input parameters used in all computer runs, regardless of the supply pressure and input heat flux, are listed in Table 6. Table 7 is a diagram of the test matrix showing the 15 combinations of input parameters used to get analytical solutions. The computed results are listed in Table 8. Calculated values for the liquid's thermal conductivity, density, and kinematic viscosity for each solution were examined to check the accuracy of the polynomial approximations at values between the points used in the derivation of their expressions. These checks uncovered no significant discrepancies between the calculated and the known values. Of all the data available from the computer solutions, the information of primary interest is that which can be directly compared to the experimental results, the ice melt velocity, and the liquid bulk temperature. Figure 22 shows the predicted relationships between the ice melt velocity and the input heat flux for the three supply pressures. The liquid bulk temperature relationship is illustrated in Figure 23. Increasing supply pressures are predicted to have only a small effect on the ice melt rate and liquid bulk temperature for a given input heat flux. This behavior is consistent with that determined experimentally. Direct comparison of the experimental results to the analytical predictions follows later in the chapter.

The preceding results were obtained by use of an expression for frictional losses in the pressure drop equation based on liquid flow between parallel plates. Because of the mass addition present at the

Table 6. Constant Input Data.

DEFINITION	SYMBOL	VALUE
FLUID EXIT PRESSURE	PE	0.1 MPa
INITIAL ICE TEMPERATURE	TI	$-17.8^{o}C$
ICE SPECIFIC HEAT	CPS	$1.964\ J/g\text{-}^{o}C$
WATER SPECIFIC HEAT	CPL	$4.187\ J/g\text{-}^{o}C$
ICE DENSITY	RHOS	$908.4\ kg/m^{3}$
ICE MELT TEMPERATURE	TM	$0^{o}C$
WATER LATENT HEAT OF FUSION	HLS	334.3 J/g
ACCEPTABLE FORCE ERROR	FERR	2.22 N
SYSTEM EXIT RADIUS	RE	15.85 mm
COEFFICIENTS FOR	AAK	$1002.1\ kg/m^{3}$
LIQUID WATER DENSITY	BBK	-2.469×10^{-1}
POLYNOMIAL	CCK	-1.666
APPROXIMATION	DDK	7.119×10^{-2}
COEFFICIENTS FOR		m^{2}/sec
LIQUID WATER	AK	1.791×10^{-6}
KINEMATIC VISCOSITY	BK	-9.755×10^{-7}
POLYNOMIAL	CK	2.632×10^{-7}
APPROXIMATION	DK	-2.496×10^{-8}
COEFFICIENTS FOR		$W/m\text{-}^{o}C$
LIQUID WATER	EK	0.566
THERMAL CONDUCTIVITY	FK	3.619×10^{-2}
POLYNOMIAL	GK	-2.983×10^{-3}
APPROXIMATION	HK	3.115×10^{-5}
NUMBER OF RADIAL LOCATIONS DESIRED	N	20
REFERENCE (4, 20, 23, 24)		

Table 7. Analytical Test Matrix, Input Data.

SUPPLY PRESSURE (MPa)	INPUT HEAT FLUX (MW/m^2)	STARTING ICE MELT VELOCITY (mm/sec)	CONVERGENCE CONSTANT (NONDIMENSIONAL)
1.269	1.262	3.302	800
	2.523	6.604	400
	3.785	9.398	200
	5.046	11.684	100
	6.308	13.716	60
2.592	1.262	3.302	800
	2.523	6.604	400
	3.785	9.652	200
	5.046	12.192	100
	6.308	14.224	60
3.606	1.262	3.302	800
	2.523	6.604	400
	3.785	9.652	200
	5.046	12.192	100
	6.308	14.224	60

Table 8. Output Data List.

ITEM	UNITS	ITEM	UNITS
ICE MELT VELOCITY	mm/sec	INITIAL ICE TEMPERATURE	^{o}C
INPUT HEAT FLUX	MW/m^2	SUPPLY PRESSURE	MPa
EXIT PRESSURE	MPa	TOTAL FORCE	N
LIQUID BULK TEMPERATURE	^{o}C	*HEAT TRANSFER* COEFFICIENT	$W/m^2\text{-}^{o}C$
LIQUID FILM THICKNESS	mm	LIQUID WATER DENSITY	kg/m^3
LIQUID WATER KINEMATIC VISCOSITY	m^2/sec	LIQUID WATER THERMAL CONDUCTIVITY	$W/m\text{-}^{o}C$

RADIAL LOCATION (mm)	LIQUID BULK VELOCITY (mm/sec)	LIQUID PRESSURE (MPa)
0.0	X	X
⋮	⋮	⋮
RE	X	X

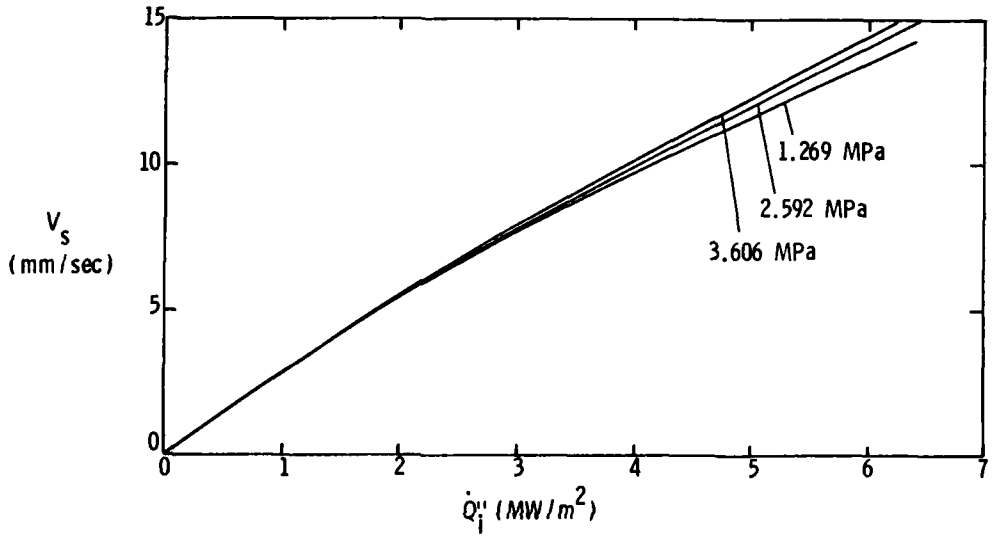

Figure 22. Analytical Results, V_s versus $\dot{Q}_i''$.

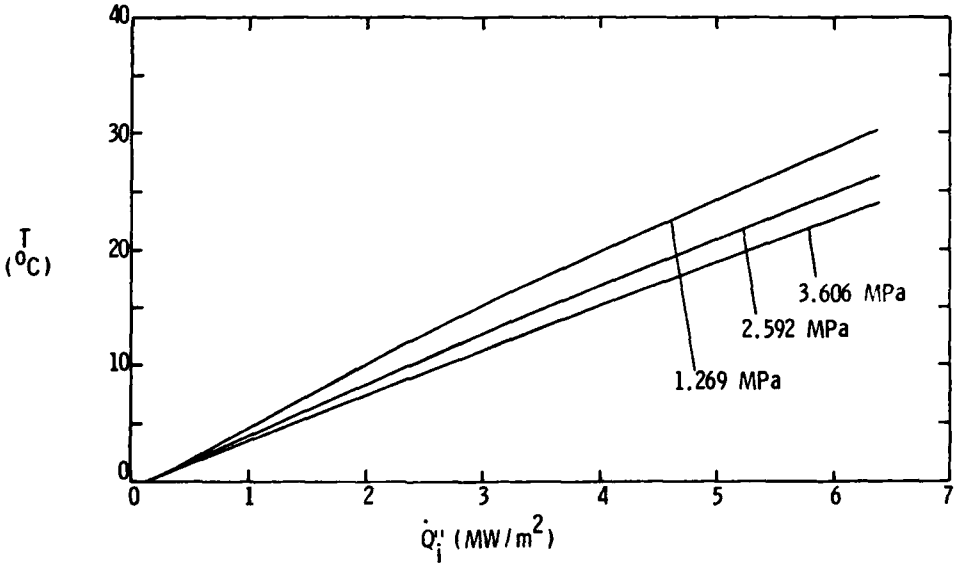

Figure 23. Analytical Results, T versus $\dot{Q}_i''$.

ice surface, this method of calculating the pressure drop is not completely accurate. To provide an alternate analytical model solution demonstrating this mass addition effect, one must revise the frictional loss term in the pressure drop equation to reflect frictional losses on the ice being one-third those on the hot block. An increase of only 1.8% for the melt velocity and a decrease of only 5% for the liquid bulk temperature at an input heat flux of 6.308 MW/m^2 (2 x 10^6 $Btu/hr\text{-}ft^2$) and a supply pressure of 3.606 MPa is predicted on the corresponding estimates for the model having equal frictional losses on both surfaces.

Of interest in determining the validity of the analytical model is the pressure distribution in the liquid film predicted by the model. Figure 24 shows the liquid pressure as a function of radial distance for a supply pressure of 2.592 MPa and an input heat flux of 3.784 MW/m^2 (1.2 x 10^6 $Btu/hr\text{-}ft^2$). This information is helpful in predicting the location of any possible boiling phenomenon that may occur in the liquid film. Figure 25 illustrates the saturation pressure-temperature relationship for water over the ranges of pressure and temperature considered in this study (25). A comparison can be made between the saturation temperature and those liquid bulk temperatures measured experimentally when the predicted pressure distribution for the liquid film is used and when the corresponding saturation temperature at a desired pressure in Figure 25 is found. The resulting conclusion of this exercise is that boiling should not have been present for all tests conducted since neither the liquid bulk temperature nor the hot block temperature near the block/liquid interface was even near 100°C during a steady state segment of data.

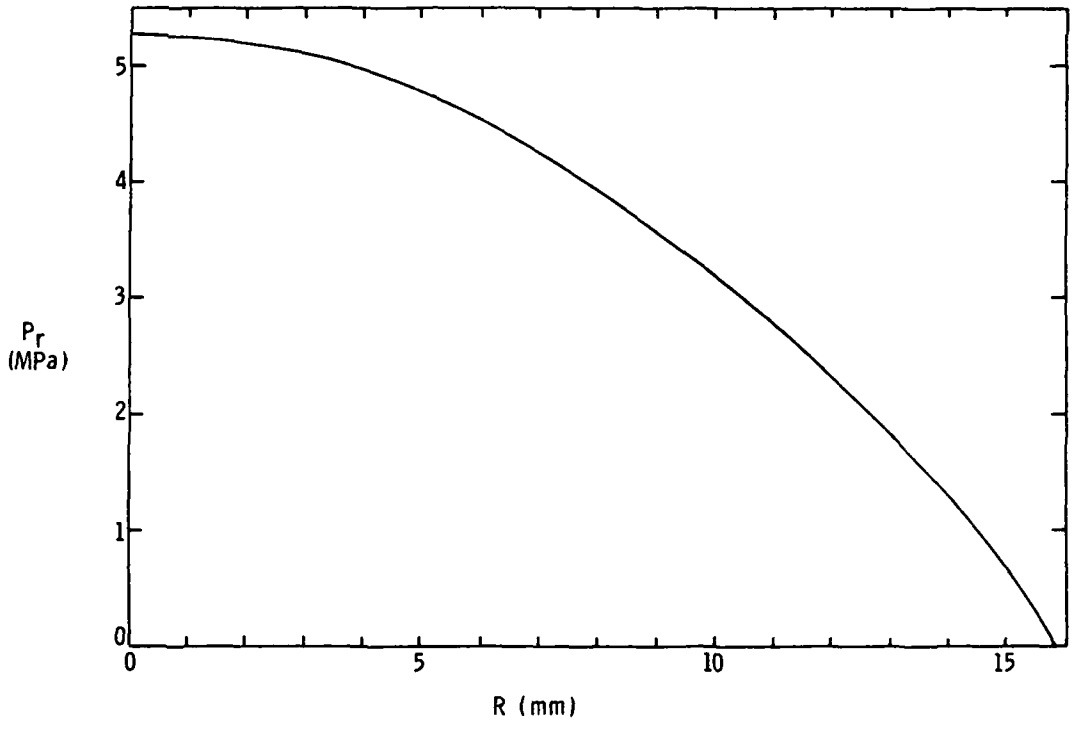

Figure 24. Predicted Pressure Distribution, P_s = 2.592 MPa, $\dot{Q}''_i$ = 3.785 MW/m^2.

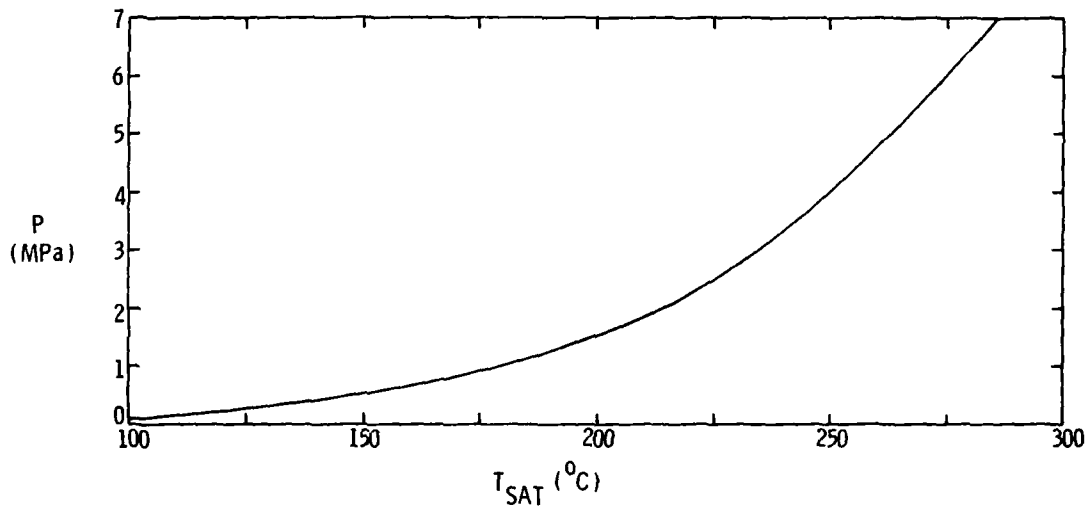

Figure 25. Pressure versus Saturation Temperature for Water.

4.3 Experimental-Analytical Comparisons

Figures 26 and 27 give a direct comparison of the ice melt velocity variation with the input heat flux as determined experimentally versus the model predictions. The two solid lines in the figures are the least squares approximation for the experimental data and indicate the two regime behavior. The broken curves represent the analytical results. The model predictions agree rather well with the experimental curves and provide a conservative estimate of the ice melt velocity for a given input heat flux and supply pressure when compared to the test data recorded after the occurrence of an anomaly. Comparison of the theoretical values to the slower rate test results are inconclusive in that only the magnitude of the ice melt performance degradation caused by the presence of some indeterminate mechanism is indicated. This mechanism is not included in the development of the analytical model. The model predicts little supply pressure influence on the ice melt velocity. This same characteristic was seen in the rapid rate experimental results.

A comparison between the predicted and measured values of the liquid bulk temperature is shown in Figures 28 and 29, The two solid lines in the figures are the least squares approximation to the bulk temperature experimental data for the same tests illustrated in Figures 26 and 27.

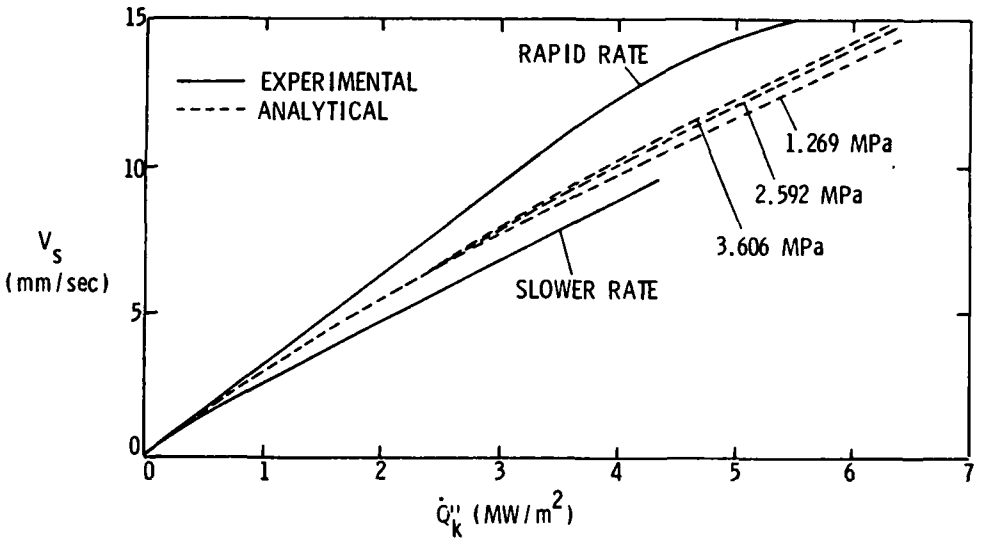

Figure 26. Experimental-Analytical Comparisons, V_s versus $\dot{Q}''_k$.

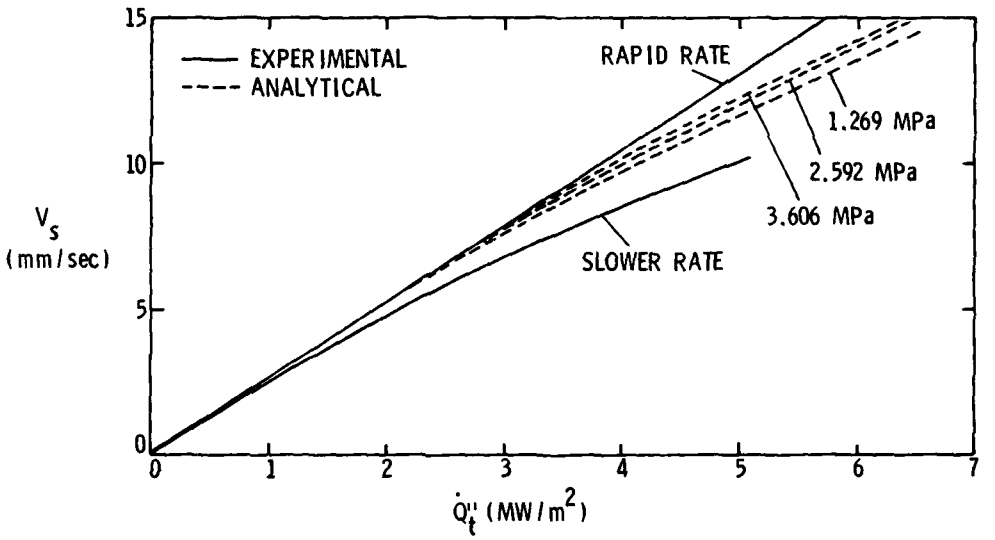

Figure 27. Experimental-Analytical Comparisons, V_s versus $\dot{Q}''_t$.

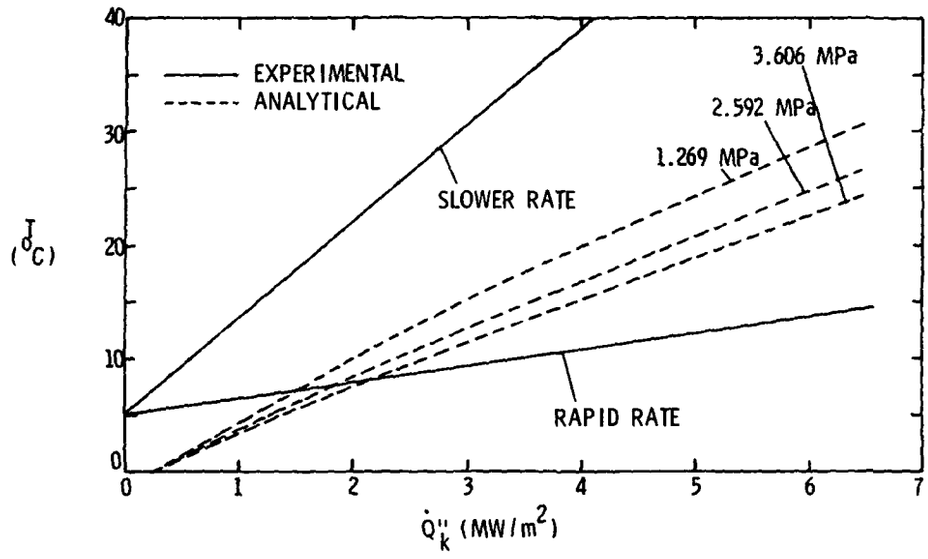

Figure 28. Experimental-Analytical Comparisons, T versus $\dot{Q}''_k$.

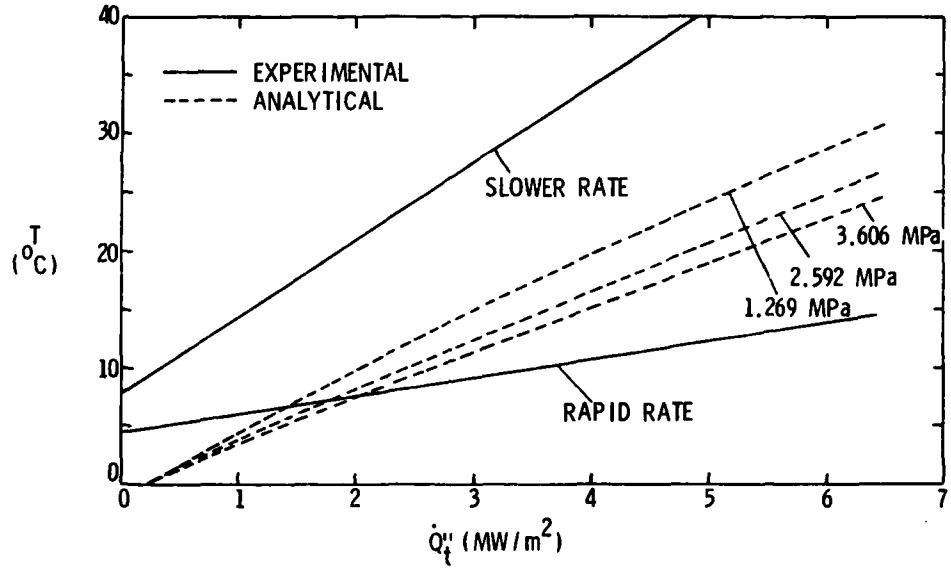

Figure 29. Experimental-Analytical Comparisons, T versus $\dot{Q}''_t$.

CHAPTER V

CONCLUSIONS AND RECOMMENDATIONS FOR FUTURE WORK

When compared with the post-anomaly test behavior, the analytical model consistently underestimates the ice melt velocity and overpredicts the liquid bulk temperature for a given input heat flux and supply pressure. These conservative estimates are within 13% of the least squares approximation of the experimental data which defines the ice melt rates for the same conditions. The liquid bulk temperature is overpredicted by no more than 33% of the least squares approximation of the experimental results for the same input heat flux and supply pressure. Because the predictions are conservative and reasonably accurate, the present analytical model can be used to safely forecast the rapid ice melt performance of a cylindrical specimen having only radially exiting liquid flow.

Prediction error for the analytical model is linked to the validity of the assumptions made in the formulation of the model. It is assumed that the distilled water used contained no dissolved air. Dissolved air is observed in the ice specimens tested. All other things being equal, air pockets uniformly dispersed in the crystalline structure of the ice tend to allow the ice to melt more quickly than a perfectly pure test sample giving a greater ice melt velocity than the model would predict. The density and specific heat of the ice are evaluated at -17.8°C (0°F). During melting, an axial temperature gradient must exist in the solid between its initial temperature and its melting temperature. Some error

may have been introduced because of this temperature discrepancy. The specific heat for the liquid is evaluated at 10°C (50°F). Experimental values for the liquid bulk temperature range between 4.4°C (40°F) and 4.1.1°C (106°F). The specific heat values at these temperatures for pure water are 4.21 J/g-°C (1.005 Btu/lbm-°F) and 4.17 J/g-°C (0.997 Btu/lbm-°F), respectively. This is only a maximum deviation of 0.5% from the assumed value and probably does not account for any major differences. It also was assumed that the liquid flow was laminar. Recalling the equation for the Reynolds number, Equation (33), and also using the predicted values for the liquid film thickness and liquid bulk velocity at the exit radius for the fastest ice melt velocity yields a Reynolds number of 231. A value of 2,000 is normally accepted as the transition point to turbulent flow in ducts (20). When it is assumed that the differences between the flow in the subject model geometry and duct flow do not result in an order of magnitude decrease in this transition value, the liquid flow of this study can be considered laminar. For the most part, the assumptions made seem to be valid and should have only a limited effect on the accuracy of the model predictions. Of those mentioned, the air content assumption probably is the only item whose effect could be significant.

The expressions from which the equations for the liquid film thickness and frictional pressure drop were developed are also probable sources of error in describing the liquid flow for the analytical model. The relations used to derive the frictional pressure drop term are for fully developed incompressible flow in a duct. The liquid film thickness equation is based on an expression for the Nusselt number described by the flow between heated parallel plates rather than the

radial outward flow present in this study. Development of the expression for δ assumes fully developed velocity and temperature profiles in the liquid. The temperature profile is fully developed. The velocity profile, on the other hand, cannot be considered fully developed since there is mass addition to the flowing liquid.

The experimental investigation contained several sources of error which influenced the accuracy of the test results. The thermocouple spacing in the hot block could only be measured within a 9% tolerance. The thermocouple placement, calibration procedures, and eventual interpretation of the recorded data all include a certain level of uncertainty. All of these error sources influenced the accuracy of the measurement system and created a total uncertainty level of about 15%. The presence of air in the ice specimens, however, and the geometry of the test network had the most pronounced effect on the test results and caused degraded melting performance on many of the tests.

The analytical predictions and the test results do concur on several points. They both show the ice melt velocity increasing to nearly the same levels as the supply pressure and input heat flux are increased. Also, they both demonstrate the same effect of increasing supply pressure on the ice melt velocity. For a given input heat flux, the ice melt velocity increases as the supply pressure is increased. The magnitude of change in ice melt velocity for constant change in supply pressure decreases as the supply pressure level increases. This indicates a diminishing returns type of relationship.

Future work on this rapid ice melting phenomenon should include improvements on the analytical model and in the design and operation of a truly steady state test rig. A better understanding of the actual

heat exchange mechanism at the heated surface should be sought. This would result in better relationships involving the fluid dynamics and heat transfer in the liquid film. The expressions for the Nusselt number (Equation (22)) and the frictional effects (Equations (31) and (32)) are only approximations to the actual flow conditions. A more detailed representation of the liquid flow, possibly using Navier-Stokes equations, may provide helpful information in more accurately modeling the system. In an effort to remove the present anomaly, test rig designs should more closely consider the effects of two-dimensional heat transfer routes, and air-free ice specimens should be used in the testing. Alternative flow exit paths and increased test specimen diameters should also be investigated in an attempt to increase the ice melt velocity capabilities.

BIBLIOGRAPHY

1. "Optimum Working Fluids for Automotive Rankine Engines, Volumes I-IV," Prepared for U. S. Environmental Protection Agency by Monsanto Research Corporation under Contract No. 68-04-0030 to Sundstrand Aviation, NTIS PB 239 247, June 1973.

2. Wolgemuth, C. H., Personal communication, State College, Pennsylvania, March 30, 1976.

3. Bankoff, S. G., "Heat Conduction or Diffusion with Change of Phase," Advances in Chemical Engr., Academic Press, New York, pp. 75-150, 1964.

4. Holman, J. P., Heat Transfer, McGraw-Hill Book Company, New York, 1972.

5. Landau, H. G., "Heat Conducting in a Melting Solid," Quarterly of Applied Mathematics, Vol. 8, pp. 81-94, 1950.

6. Lotkin, M., "The Calculation of Heat Flow in Melting Solids," Quarterly of Applied Mathematics, Vol. 18, pp. 79-85, April 1960.

7. Musman, S., "Penetrative Convection," J. of Fluid Mechanics, Vol. 31, Part 2, pp. 343-360, 1968.

8. Yen, Yin-Chao, "Natural Convection in Ice Melting from Below," Cold Regions Research & Engineering Laboratory, Hanover, New Hampshire, December 1966.

9. Yen, Yin-Chao, "Analytical and Experimental Study of a Melting Problem with Natural Convection," Cold Regions Research & Engineering Laboratory, Hanover, New Hampshire, July 1967.

10. Moore, D. R., and N. O. Weiss, "Nonlinear Penetrative Convection," J. of Fluid Mechanics, Vol. 61, Part 3, pp. 553-581, 1973.

11. Yen, Yin-Chao, "Therman Instability in a Layer of Water Formed by Melting Ice from Below," Cold Regions Research & Engineering Laboratory, Hanover, New Hampshire, March 1969.

12. Bowley, W. W., "Two-Dimensional Melting in a Channel," Ph.D. Thesis, The University of Connecticut, 1965.

13. Friedman, E., "An Iterative Procedure for Including Phase Change in Transient Heat Conduction Programs and Its Incorporation into the Finite Element Method," Submitted through AIChE HT & EC Division for 1977 National Heat Transfer Conference.

14. Murray, W. D., and F. Landis, "Numerical and Machine Solutions of Transient Heat Conduction Problems Involving Melting or Freezing," J. of Heat Transfer, ASME Trans. Series C, Vol. 81, pp. 106-112, 1959.

15. Nansteel, M. W., "An Investigation of a Two-Phase, Moving Boundary System, with Convection at the Solid-Liquid Interface," The Pennsylvania State University, M.S. Thesis, May 1979.

16. Kreith, F., and F. E. Romie, "A Study of the Thermal Diffusion Equation with Boundary Conditions Corresponding to Solidification or Melting of Materials Initially at the Fusion Temperature," Proceedings of Physics Society, Vol. 68, pp. 277-291, 1955.

17. Yen, Yin-Chao, and Chi Tien, "A Theoretical Investigation on the Effects of Melting on Forced Convection Heat Transfer," Cold Regions Research & Engineering Laboratory, Hanover, New Hampshire, October 1965.

18. Masters, J. I., "Problem of Intense Surface Heating of a Slab Accompanied by Change of Phase," J. of Applied Physics, Vol. 27, p. 477, 1956.

19. Kays, W. M., Convective Heat and Mass Transfer, McGraw-Hill Book Company, New York, p. 115, 1966.

20. Olson, R. M., Essentials of Engineering Fluid Mechanics, Third Edition, Intext Educational Publishers, New York.

21. The Omega 1977 Temperature Measurement Handbook, Omega Engr. Inc., Stamford, Connecticut, p. A-4, 1977.

22. Taylor, L., ed., Metals Handbook, Eighth Edition, Vol. 1, American Society for Metals, Metals Park, Novelty, Ohio, p. 102, 1961.

23. Marks, L. S., Mechanical Engineers Handbook, Fifth Edition, McGraw-Hill Book Company Inc., New York, p. 281, 1951.

24. Murphy, D. B., and V. Rousseau, Foundations of College Chemistry, The Ronald Press Company, New York, p. 234, 1969.

25. Sonntag, R. E., and G. J. VanWylen, Introduction to Thermodynamics Classical and Statistical, John Wiley & Sons Inc., New York, 1971.

26. Comini, G., and others, "Finite Element Solutions of Non-Linear Heat Conduction Problems with Special Reference to Phase Change," International J. for Numerical Methods in Engineering, Vol. 8, No. 3, p. 613-624, 1974.

27. Price, P. H., and M. R. Slack, "The Effect of Latent Heat on Numerical Solutions of the Heat Flow Equation," British J. of Applied Physics, Vol. 5, pp. 285-287, August 1954.

28. Dankwertz, P. V., "Unsteady State Diffusion of Heat Conduction with Moving Boundaries," Trans. Faraday Society, Vol. 46, No. 333, pp. 701-712, 1950.

29. Stubstad, J., W. F. Quinn, and Yin-Chao Yen, "Melting Heat Transfer and Flow Characteristics of an Ice-Water Heat Sink," Submitted through AIChE HT & EC Division for 1977 National Heat Transfer Conference.

30. Muehlbauer, J. C., and J. E. Sunderland, "Heat Conduction with Freezing or Melting," Applied Mechanics Reviews, Vol. 18, No. 12, pp. 951-959, December 1965.

31. Boley, B. A., "The Analysis of Problems of Heat Conduction and Melting," High Temperature Structures and Materials; Proceedings of the Third Symposium on Naval Structural Mechanics, Pergamon Press, pp. 260-365, 1963.

32. Ozisik, M. N., Boundary Value Problems of Heat Conduction, International Textbook Company, Scranton, Pennsylvania, 1968.

33. Schlicting, H., Boundary Layer Theory, McGraw-Hill Book Co., Inc., New York, 1955.

34. Riddle, D. F., Calculus and Analytical Geometry, Wadsworth Publishing Company, Belmont, California, 1970.

35. Jakob, M., Heat Transfer, John Wiley & Sons Inc., Vol. 1, New York, 1956.

36. Carslaw, H. S., and J. C. Jaeger, Conduction of Heat in Solids, Oxford University Press, Amen House, London E. C. 4, pp. 282-296, 1960.

37. Ford, T. J., "Enhancement of Rates of Freezing and Melting in the Programmed Indirect Freezing Process," University of Denver, Ph.D. Thesis, February 1975.

38. Spotts, M. F., Design of Machine Elements, Fourth Edition, Prentice-Hall Inc., Englewood Cliffs, New Jersey, 1971.

39. Beckett, R., and J. Hurt, Numerical Calculations and Algorithms, McGraw-Hill Book Company, New York, 1967.

40. Benedict, R. P., Fundamentals of Temperature, Pressure, and Flow Measurements, Second Edition, John Wiley & Sons, New York, 1977.

41. Eckert, E. R. G., and R. M. Drake, Jr., Analysis of Heat and Mass Transfer, McGraw-Hill, New York, p. 222, 1972.

APPENDIX A

DERIVATION OF THE POLYNOMIAL APPROXIMATIONS FOR THE KINEMATIC VISCOSITY, DENSITY, AND THERMAL CONDUCTIVITY OF WATER AS A FUNCTION OF LIQUID BULK TEMPERATURE

AD-A089 099 PENNSYLVANIA STATE UNIV UNIVERSITY PARK APPLIED RESE--ETC F/G 7/4
AN INVESTIGATION OF THE HEAT TRANSFER AT THE LIQUID/SOLID INTER--ETC(U)
MAR 80 J E FREDLEY N00024-79-C-6043
UNCLASSIFIED ARL/PSU/TM-80-94 NL

2 to 2

END
DATE FILMED
10-80
DTIC

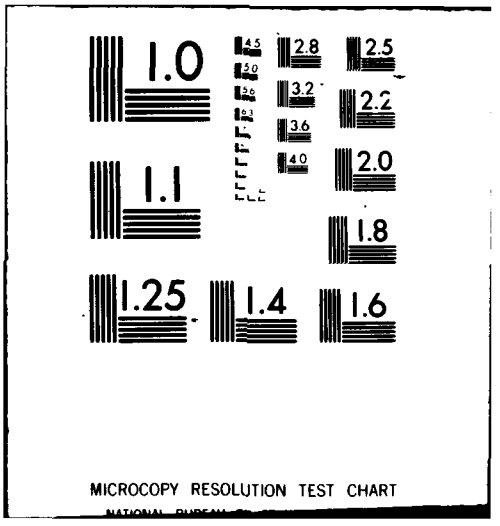
1.0
1.1
1.25
1.4
1.6
1.8
2.0
2.2
2.5
2.8
3.2
3.6
4.0
MICROCOPY RESOLUTION TEST CHART

A survey of the change in water properties between the temperatures $0^{o}C$ ($32^{o}F$) and $93.3^{o}C$ ($200^{o}F$) indicates that the density, thermal conductivity, and particularly the kinematic viscosity vary significantly. Because the range of liquid bulk temperatures generated by the computer solution are not known a priori, the above properties are approximated as a function of the liquid bulk temperature using a polynomial expression.

The properties are approximated as a function of temperature by use of a third order polynomial of the form below:

$$\text{Property} = A + B\bar{T} + C\bar{T}^{2} + D\bar{T}^{3} \quad . \tag{A.1}$$

The variable $\bar{T}$ is the liquid bulk temperature nondimensionalized by the melt temperature.

$$\bar{T} = \frac{T - T_{m}}{T_{m}} \quad . \tag{A.2}$$

Values for $\bar{T}$ for liquid bulk temperatures of $0^{o}C$ ($32^{o}F$), $15.6^{o}C$ ($60^{o}F$), $37.8^{o}C$ ($100^{o}F$), and $93.3^{o}C$ ($200^{o}F$) are evaluated and associated with the property value corresponding to the T. The Fahrenheit values were used to avoid division by zero in Equation (A.2). The four constants A, B, C, and D can be evaluated by use of the four selected values for $\bar{T}$ and their corresponding property values. This then provides a method of evaluating the necessary water properties as a function of temperature.

APPENDIX B

TABULATION OF THE RAW TEST DATA

Table B-1. Raw Test Data, P_s = 1.269 MPa.

Run No.	Initial Hot Block Temperature (°C)	Time Interval (sec)	Ice Position (cm)	Hot Block Temperature (°C)	Hot Block Temperature (°C)	Liquid Bulk Temperature (°C)	Liquid Bulk Temperature (°C)
52	237.8	2.48 - 6.48	14.22 - 17.53	72.8	43.9	36.1	41.1
53A	93.3	5.80 - 15.48	11.18 - 14.22	27.8	17.8	12.2	12.2
53B	93.3	20.20 - 29.80	15.75 - 18.54	21.7	12.8	12.2	11.1
54	171.1	3.84 - 9.04	14.32 - 17.78	50.6	30.6	negl. flow	22.2
55	260.0	2.16 - 4.64	14.97 - 17.27	80.6	48.9	37.8	42.8
56A	193.3	1.80 - 3.52	13.72 - 15.24	63.3	42.2	23.3	negl. flow
56B	193.3	4.60 - 7.12	16.26 - 18.79	50.6	26.7	12.2	negl. flow
57A	65.6	4.40 - 12.20	8.64 - 10.92	22.2	13.9	negl. flow	18.9
57B	65.6	13.28 - 32.40	11.18 - 15.49	17.2	11.1	negl. flow	12.2
58	215.6	2.68 - 10.56	11.68 - 17.27	63.3	39.4	34.4	33.3
59A	193.3	3.72 - 7.32	12.70 - 15.24	62.8	38.9	37.8	30.6
59B	193.3	8.00 - 11.12	15.75 - 18.29	57.8	38.9	21.1	26.1
60	148.9	3.40 - 12.80	13.21 - 17.78	44.4	27.8	23.9	25.0
61	171.1	2.16 - 8.56	12.19 - 15.75	53.3	32.8	32.8	26.1
62	215.6	2.40 - 6.12	13.72 - 16.76	71.1	42.8	37.8	34.4
63	193.3	2.12 - 8.56	13.21 - 17.78	63.9	38.9	negl. flow	33.9

Table B-2. Raw Test Data, P_s = 2.592 MPa.

Run No.	Initial Hot Block Temperature (°C)	Time Interval (sec)	Ice Position (cm)	Hot Block Temperature (°C)	Hot Block Temperature (°C)	Liquid Bulk Temperature (°C)	Liquid Bulk Temperature (°C)
37	121.1	4.32 - 10.24	12.70 - 16.76	27.9	10.0	9.4	6.7
38	104.4	4.04 - 11.24	12.70 - 17.27	26.1	9.4	7.2	8.9
39A	71.1	3.76 - 13.00	9.65 - 13.21	17.8	10.6	negl. flow	8.9
39B	71.1	20.88 - 28.96	16.26 - 18.79	12.2	5.0	negl. flow	4.4
40	260.0	1.92 - 3.28	16.26 - 18.29	60.0	19.4	12.2	13.3
41A	121.1	4.52 - 6.92	11.68 - 13.21	29.4	12.8	8.3	10.6
41B	121.1	10.36 - 15.32	15.24 - 18.29	23.3	8.9	7.2	7.2
42A	60.0	3.80 - 13.20	10.67 - 13.21	7.8	3.3	5.0	negl. flow
42B	60.0	28.88 - 42.08	16.00 - 17.78	3.3	1.7	4.4	negl. flow
44	232.2	2.24 - 4.08	16.26 - 18.79	56.7	21.1	10.0	10.0
45	171.1	2.60 - 4.44	15.24 - 17.27	43.9	17.8	negl. flow	5.0
46	221.1	2.80 - 4.84	15.24 - 17.78	53.9	20.6	11.1	negl. flow
47A	193.3	1.68 - 5.24	13.21 - 16.26	57.8	29.5	27.9	negl. flow
47B	193.3	6.88 - 7.76	17.78 - 18.79	42.2	12.8	8.3	21.1
48	171.1	3.16 - 5.92	15.75 - 18.29	35.0	14.4	6.7	7.2
49	260.0	2.60 - 4.00	16.76 - 18.79	57.2	20.0	10.0	11.1
50A	260.0	1.68 - 3.76	14.22 - 16.76	72.2	39.4	18.3	19.4
50B	260.0	4.28 - 5.36	17.53 - 19.05	60.6	26.1	14.4	10.6
51	237.8	1.92 - 5.08	14.32 - 18.79	57.2	21.7	12.8	11.7

Table B-3. Raw Test Data, P_s = 3.606 MPa.

Run No.	Initial Hot Block Temperature (°C)	Time Interval (sec)	Ice Position (cm)	Hot Block Temperature (°C)	Hot Block Temperature (°C)	Liquid Bulk Temperature (°C)	Liquid Bulk Temperature (°C)
64	237.8	2.32 - 4.68	15.75 - 18.79	53.3	17.8	15.0	16.1
65A	93.3	3.80 - 8.40	11.68 - 14.22	21.7	8.9	6.7	12.8
65B	93.3	12.72 - 19.00	16.26 - 18.79	16.7	6.1	7.8	8.9
66A	171.1	2.24 - 4.44	14.22 - 15.75	50.0	26.7	33.9	30.6
66B	171.1	5.44 - 7.08	17.27 - 18.79	35.0	11.7	12.2	8.9
67	260.0	2.00 - 3.00	17.27 - 18.79	64.4	21.7	14.4	13.3
68A	148.9	1.84 - 6.04	12.70 - 16.80	45.0	24.4	25.6	27.8
68B	148.9	7.72 - 9.64	17.53 - 19.05	31.1	10.0	8.3	7.2
69A	65.6	3.28 - 9.08	11.18 - 13.72	15.0	4.4	negl. flow	5.6
69B	65.6	13.16 - 21.28	15.24 - 17.78	11.1	3.3	negl. flow	5.6
70	260.0	3.08 - 4.44	16.26 - 18.29	67.2	26.1	negl. flow	10.0
71	215.6	2.24 - 3.72	16.26 - 18.29	51.7	20.0	negl. flow	11.7
72	193.3	2.12 - 4.00	16.51 - 18.54	42.2	15.0	10.6	14.4
73	237.8	1.88 - 4.00	15.75 - 18.79	60.6	21.1	16.7	13.9
74	182.2	2.52 - 4.96	16.26 - 18.79	38.3	13.9	10.6	11.1
75	215.6	1.72 - 3.60	16.26 - 18.79	52.8	18.3	11.1	11.7

DISTRIBUTION

Commander (NSEA 09G32)
Naval Sea Systems Command
Department of the Navy
Washington, DC 20362 — Copies 1 and 2

Commander (NSEA 0342)
Naval Sea Systems Command
Department of the Navy
Washington, DC 20362 — Copies 3 and 4

Defense Technical Information Center
5010 Duke Street
Cameron Station
Alexandria, VA 22314 — Copies 5 through 16